PNL-6049 Vol. I
UC-85

COBRA-SFS: A Thermal-Hydraulic Analysis Computer Code

Volume I: Mathematical Models and Solution Method

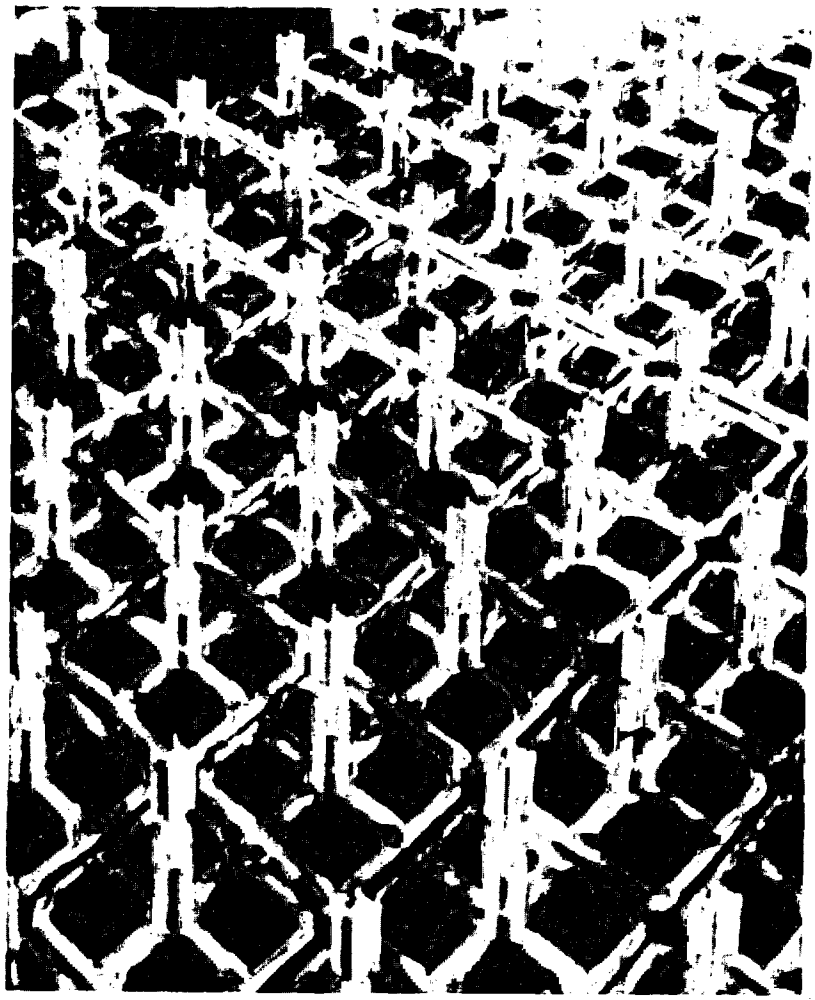

November 1986

Prepared for the U.S. Department of Energy
under Contract DE-AC06-76RLO 1830

Pacific Northwest Laboratory
Operated for the U.S. Department of Energy
by Battelle Memorial Institute

PNL-6049 Vol. I

DISCLAIMER

PACIFIC NORTHWEST LABORATORY
operated by
BATTELLE
for the
UNITED STATES DEPARTMENT OF ENERGY
under Contract DE-AC06-76RLO 1830

Printed in the United States of America
Available from
National Technical Information Service
United States Department of Commerce
5285 Port Royal Road
Springfield, Virginia 22161

NTIS Price Codes
Microfiche A01

Printed Copy

Pages	Price Codes
001-025	A02
026-050	A03
051-075	A04
076-100	A05
101-125	A06
126-150	A07
151-175	A08
176-200	A09
201-225	A010
226-250	A011
251-275	A012
276-300	A013

PNL-6049 Vol. 1
UC-85

COBRA-SFS: A THERMAL-HYDRAULIC ANALYSIS COMPUTER CODE

VOLUME 1 - MATHEMATICAL MODELS AND SOLUTION METHOD

D. R. Rector
C. L. Wheeler
N. J. Lombardo

November 1986

Prepared for
the U.S. Department of Energy
under Contract DE-AC06-76RLO 1830

Pacific Northwest Laboratory
Richland, Washington 99352

ABSTRACT

COBRA-SFS (Spent Fuel Storage) is a general thermal-hydraulic analysis computer code used to predict temperatures and velocities in a wide variety of systems. The code was refined and specialized for spent fuel storage system analyses for the U.S. Department of Energy's Commercial Spent Fuel Management Program.

The finite-volume equations governing mass, momentum, and energy conservation are written for an incompressible, single-phase fluid. The flow equations model a wide range of conditions including natural circulation. The energy equations include the effects of solid and fluid conduction, natural convection, and thermal radiation. The COBRA-SFS code is structured to perform both steady-state and transient calculations; however, the transient capability has not yet been validated.

This volume describes the finite-volume equations and the method used to solve these equations. It is directed toward the user who is interested in gaining a more complete understanding of these methods.

ACKNOWLEDGMENTS

The authors would like to thank the Department of Energy for sponsoring this work. Thanks are also extended to Darrell Newman, Dale Oden, and Gordon Beeman of Pacific Northwest Laboratory's Commercial Spent Fuel Management Program Office (CSFM-PO). The support of Jim Creer of the CSFM/Dry Storage System Performance Evaluation Project was essential to the successful completion of this documentation effort. Appreciation is extended to T. E. Michener and J. M. Cuta for their contribution to the COBRA-SFS effort. Finally, thanks to E. C. Darby, C. M. Stewart, word processors, and T. L. Gilbride, editor for their preparation of this document.

CONTENTS

FIGURES

TABLES

NOMENCLATURE

SYMBOLS AND NOTATIONS

α_i - set of slab numbers with a conduction connection to slab i

β_i - set of slab numbers with a thermal radiation connection to rod i

γ_i - set of channel numbers with a thermal connection to rod i

Δt - time step (s)

Δx - axial step (ft)

ϵ - surface emittance or a member of a set

ζ_i - set of rod numbers with a thermal radiation connection to rod i

θ - problem orientation, angle from vertical

κ_i - set of rod numbers with a thermal radiation connection to slab i

λ - thermal conductivity

λ_i - set of rod numbers with a thermal connection to subchannel i

μ - viscosity (lbm/ft s)

ξ_i - set of subchannel numbers with a thermal connection to slab i

ρ - density (lbm/ft^3)

σ - Stephan-Boltzmann constant (BTU/h $ft^2 {}^\circ R^4$)

σ_i - set of slab numbers with a thermal radiation connection to slab i

τ_i - set of slab numbers with a thermal connection to subchannel i

ϕ - area fraction

ϕ_i - rod to subchannel i heat fraction

Ψ_i - set of transverse gap connections to subchannel i

ℓ - length of transverse momentum control volume (ft)

A - area (ft^2)

c - specific heat (BTU/lbm-$^\circ$F)

C - drag, axial loss coefficient, empirical coefficient, or specific heat (BTU/lbm-°F)

D - Darcy and orifice drag

D_h - hydraulic diameter (ft)

e_ik - switch function (±1) that gives the correct sign to the transverse connection terms

f - friction factor

f_c - constant of proportion relating turbulent momentum to turbulent energy transport

F_{ij} - blackbody viewfactor

F_{ij} - radiation exchange factor, surface i to j

F_g - body force

F_s - shear force

g - acceleration due to gravity (ft/s^2)

Gr - Grashoff number

h - fluid enthalpy (BTU/lbm)

H - average film coefficient, or heat transfer coefficient ($BTU/s\text{-}ft^2\text{-}°F$)

H_g - fuel-cladding gap conductance ($BTU/s\text{-}ft^2\text{-}°F$)

k - thermal conductivity (BTU/s-ft-°F)

K - axial loss coefficient

K_G - transverse loss coefficient

L - length (ft)

m - axial flow rate (lbm/s)

Nu - Nusselt number

p,P - pressure (lbf/ft^2)

P_h - heated perimeter (ft)

P_W - wetted perimeter (ft)

Pr - Prandtl number

q" - heat flux (BTU/s ft^2)

q''' - volumetric heat generation (BTU/s ft^3)

Q_{AX} - axial heat rate (BTU/s)

Q_{FF} - fluid-to-fluid heat rate (BTU/s)

Q_{FR} - rod-to-fluid heat rate (BTU/s)

Q_{RR} - rod-to-rod heat rate (BTU/s)

Q_{RW} - rod-to-slab heat rate (BTU/s)

Q_{WW} - slab-to-slab heat rate (BTU/s)

R - radial thermal resistance, radius (ft) or flow resistance (1/ft-lbm)

r - radius (ft)

Ra - Rayleigh number

R_c - outer radius of the cladding (ft)

Re - Reynolds number

R_f - outer radius of the fuel material (ft)

S - transverse gap width (ft)

t - time (s)

t_w - effective slab thickness for heat storage (ft)

T - temperature (°F)

T_a - ambient temperature (°F)

T_c - cladding temperature (°F)

T_{fs} - temperature of the fuel surface (°F)

T_s - local surface temperature (°F)

T_{sat} - saturation temperature (°F)

T_w - slab temperature (°F)

U - axial velocity (ft/s) or effective slab conductance

$\bar{u}$ - average axial velocity in gap (ft/s)

V - transverse velocity (ft/s)

w - crossflow per unit axial length (lbm/ft-s)

w_T - crossflow due to turbulent exchange (lbm/s-ft)

y_c - cladding thickness (ft)

Z - factor for effective fluid radial conduction length

SUPERSCRIPTS

n - time step level or Nusselt number exponent

N - empirical coefficient

o - old iterate value

* - donor cell quantity

~ - tentative value

- - average value

SUBSCRIPTS

a - ambient

c - cladding or convection

D - diameter

f - friction or fuel

HTR - heat transfer from a rod

HTW - heat transfer from a wall

i - reference control volume number or generalized subscript for matrix notation

ii,jj - refer to channel numbers on either side of a transverse gap

j - axial level or generalized subscript for matrix notation

k - transverse gap number or conduction

L - length

m - wall number

n - rod number

r - radiation

R - rod

s - surface

T - transverse

w - slab

COBRA-SFS: A THERMAL-HYDRAULIC ANALYSIS COMPUTER CODE
VOLUME I - MATHEMATICAL MODELS AND SOLUTION METHOD

1.0 INTRODUCTION

COBRA-SFS (Spent Fuel Storage) is a generalized computer code developed by Pacific Northwest Laboratory (PNL)[(a)] to evaluate the thermal-hydraulic performance of a wide variety of systems. Even though the code was refined and specialized for spent fuel storage system analyses, it is designed to predict flow and temperature distributions under a wide range of flow conditions, including mixed and natural convection. The COBRA-SFS code is structured to perform both steady-state and transient calculations; however, the transient capability has not yet been validated.

COBRA-SFS is a single-phase flow computer code based on the strengths of other codes in the COBRA series (Rowe 1973; Wheeler et al. 1976; Stewart et al. 1977; George et al. 1980). The equations governing mass, momentum, and energy conservation for incompressible flows are solved using a semi-implicit method similar to that used in COBRA-WC (George et al. 1980) that allows recirculating flows to be predicted. The lumped, finite-volume nodalization used in COBRA-SFS allows a great deal of flexibility in modeling a wide variety of geometries.

In addition to many features of previous COBRA codes, COBRA-SFS has several additional features that are specific to spent fuel storage analysis:

- A solution method that calculates three-dimensional conduction heat transfer through a solid structure network such as a spent fuel cask basket or cask body
- A detailed radiation heat transfer model that calculates radiation on a detailed rod-to-rod basis

---

(a) Operated for the U.S. Department of Energy by Battelle Memorial Institute.

- Thermal boundary conditions to model radiation and natural convection heat transfer from storage system surfaces
- A total flow boundary condition that automatically adjusts the pressure field to yield the specified total flow for a system.

The documentation of the COBRA-SFS code consists of three separate volumes. In this volume, Volume I: Mathematical Models and Solution Method, the theory behind the code is described. The input instructions and guidance in applying the code are presented in Volume II: Users' Manual (Rector et al. 1986a). An extensive effort to validate the COBRA-SFS code was performed using data from single-assembly and multi-assembly storage system tests (Cuta and Creer 1986; Rector et al. 1986b; Wiles et al. 1986). Results of this effort using the documented version of COBRA-SFS are presented in Volume III: Validation Assessments (Lombardo et al. 1986).

2.0 COBRA-SFS MODELING APPROACH

The COBRA-SFS (Spent Fuel Storage) computer code can be used to evaluate the thermal-hydraulic performance of spent nuclear fuel storage systems, although it may be applied to a wide range of flow and heat transfer problems. Stored spent fuel assemblies generate decay heat that must be effectively removed to maintain temperatures within acceptable limits. In most spent fuel storage systems, the three modes of heat transfer--conduction, convection, and radiation--contribute to the removal of decay heat from the spent fuel assemblies.

A simplified sketch of a typical spent fuel dry storage cask is shown in Figure 2.1. Convection heat transfer within the cask removes decay heat by circulating fluid up through the heated spent fuel assemblies and down through the cooler regions of the cask. In addition, decay heat is removed from the assembly by conduction through the fluid and solid components and by surface-to-surface radiation. The heat is then conducted through the cask body to the cask outer surface, where it is removed by natural convection and radiation.

A typical COBRA-SFS cask model, shown in Figure 2.2, is divided into three regions: an upper plenum, a channel region, and a lower plenum. The channel region is divided into several axial levels consisting of detailed fluid, solid structure, and fuel rod nodes where the flow and temperature distribution within the cask are calculated.

The upper and lower plenums consist of regions within which the fluid is uniformly mixed. A set of thermal connections are used to describe heat transfer between the fluid in the channel region and the boundary. The plenum regions are optional and are used primarily when it is necessary to model recirculating flow and axial heat transfer.

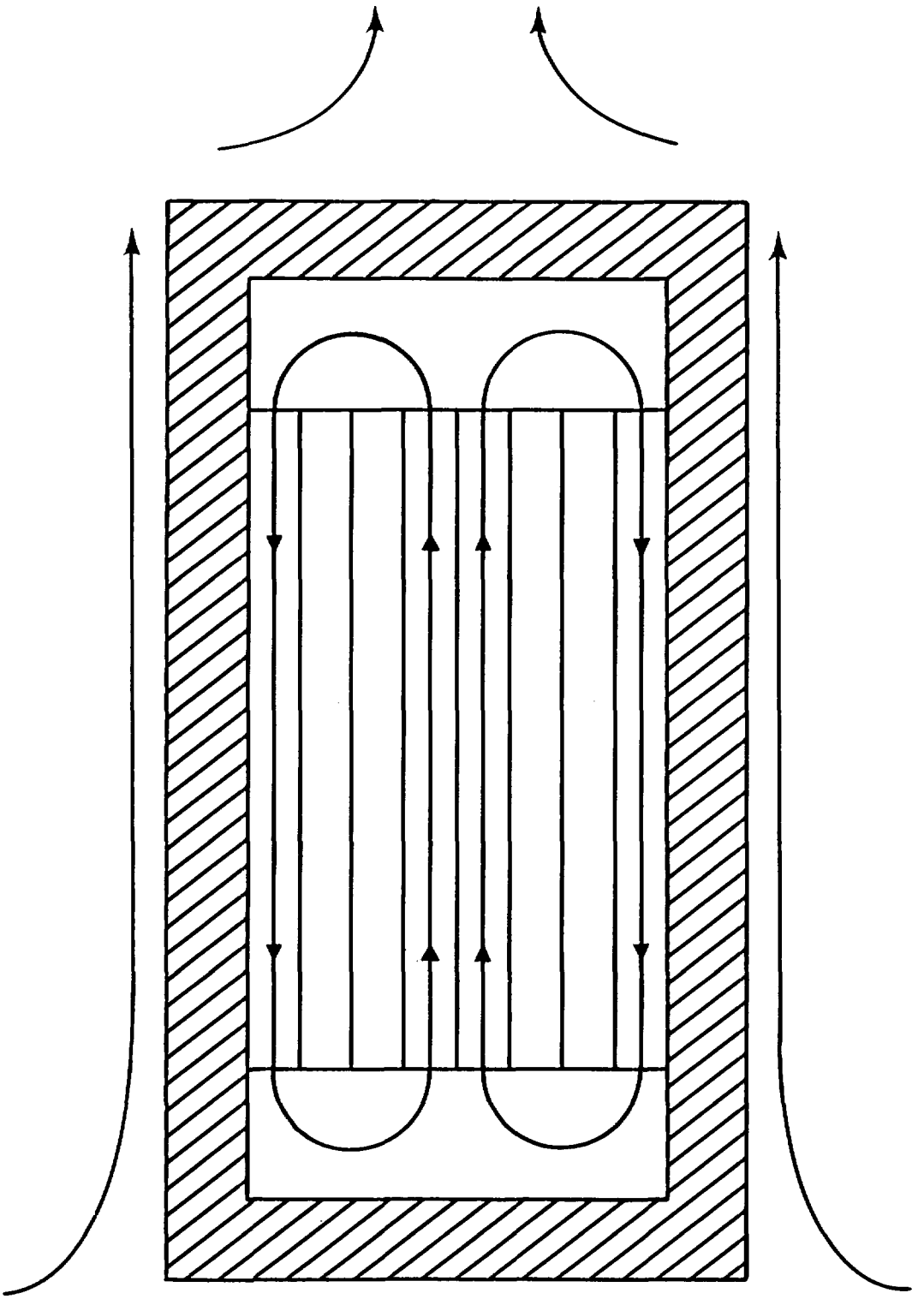

FIGURE 2.1. Cut-Away Sketch of a Typical Spent Fuel Cask

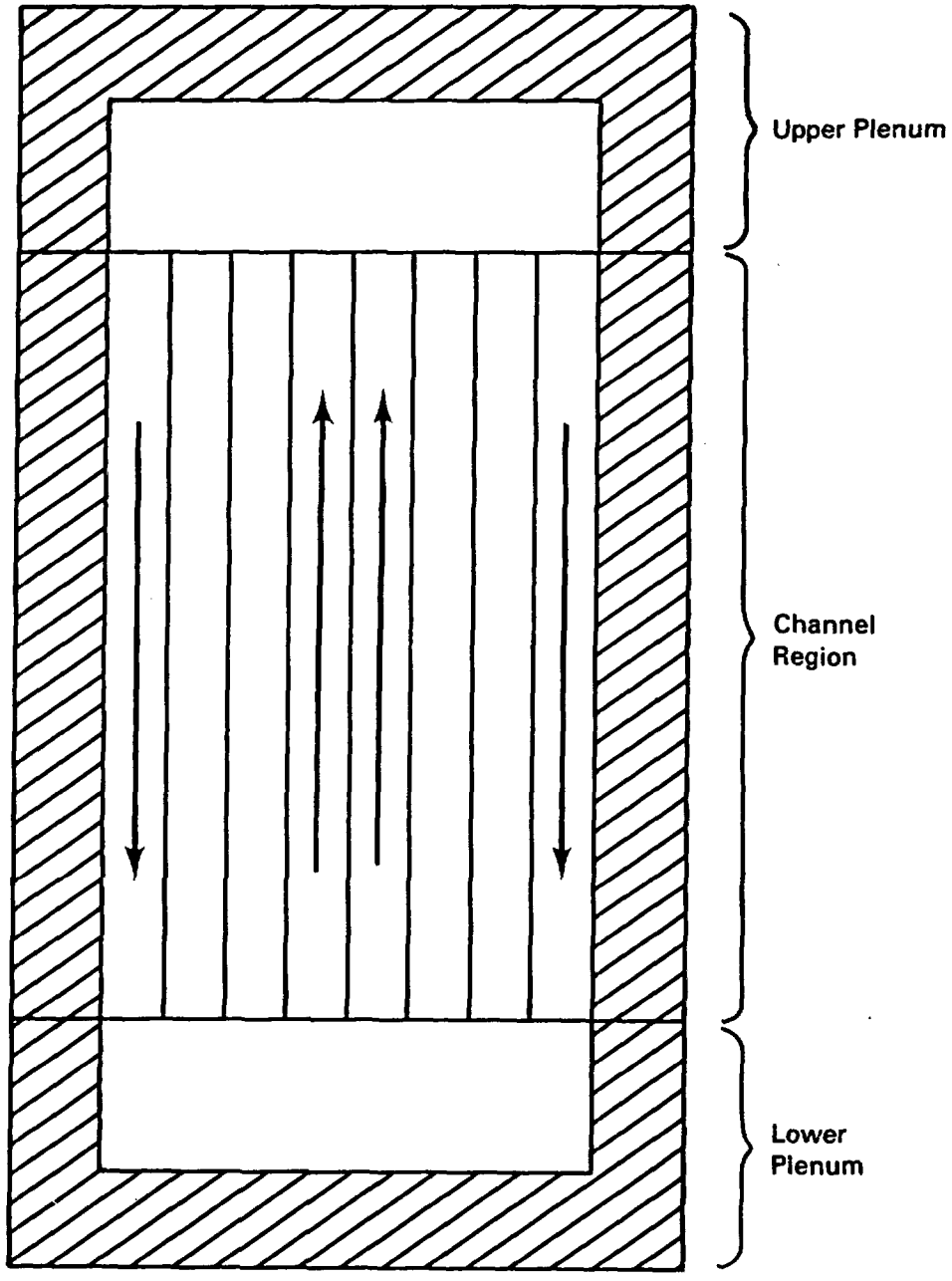

FIGURE 2.2. Typical COBRA-SFS Cask Model

To model convection heat transfer, a solution of the flow field is required. Therefore, the COBRA-SFS solution is divided into two parts--a flow field solution and an energy solution. For forced convection, these two solutions are relatively independent. However, for natural convection, these two solutions are tightly coupled. An iterative method is used to solve the combined flow field and temperature distributions. A simplified flow chart of this method is shown in Figure 2.3.

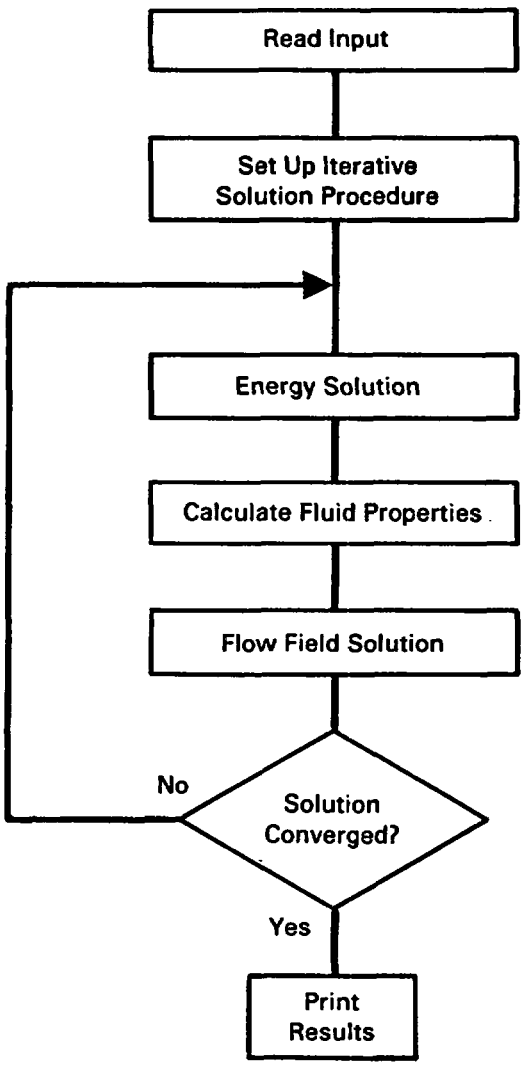

FIGURE 2.3. Simplified COBRA-SFS Flow Chart

3.0 FLOW FIELD MODELS AND SOLUTION METHOD

The COBRA-SFS code solves a set of finite-volume equations governing conservation of mass, momentum, and energy. The thermal-hydraulic analysis is separated into two parts--a flow field solution and an energy solution. In this section, the equations and method used to obtain a flow field solution are described in detail. The derivation of the conservation equations for mass, axial, and transverse momentum is demonstrated in Section 3.1. The numerical method for solving the equations is presented in Section 3.2. The constitutive models for flow resistance and turbulent mixing are presented in Section 3.3. The boundary conditions that may be applied to the flow equations are described in Section 3.4. A similar treatment of the energy solution is presented in Section 4.0.

3.1 CONSERVATION EQUATIONS

For a rod assembly stored in a vertical orientation, fluid flow is constrained by the surfaces of the closely spaced fuel rods oriented parallel to the primary flow direction. On a small scale, the fuel rods partition the flow area into many subchannels that communicate laterally by crossflow through narrow gaps. The control volume used in the development of the conservation equations is an axial segment of a subchannel as illustrated in Figure 3.1.

To derive the conservation equations, suitable balances are performed on the typical control volume shown in Figure 3.2. The axial length of the control volume is denoted by Δx. The axial flow area at the upper and lower surfaces is denoted by A and the axial velocity by U. Assuming linear variation in area between the upper and lower surfaces, the node volume is numerically equivalent to $\bar{A}\Delta x$ where $\bar{A}$ is the average axial flow area, $(A_x + A_{x-\Delta x})/2$.

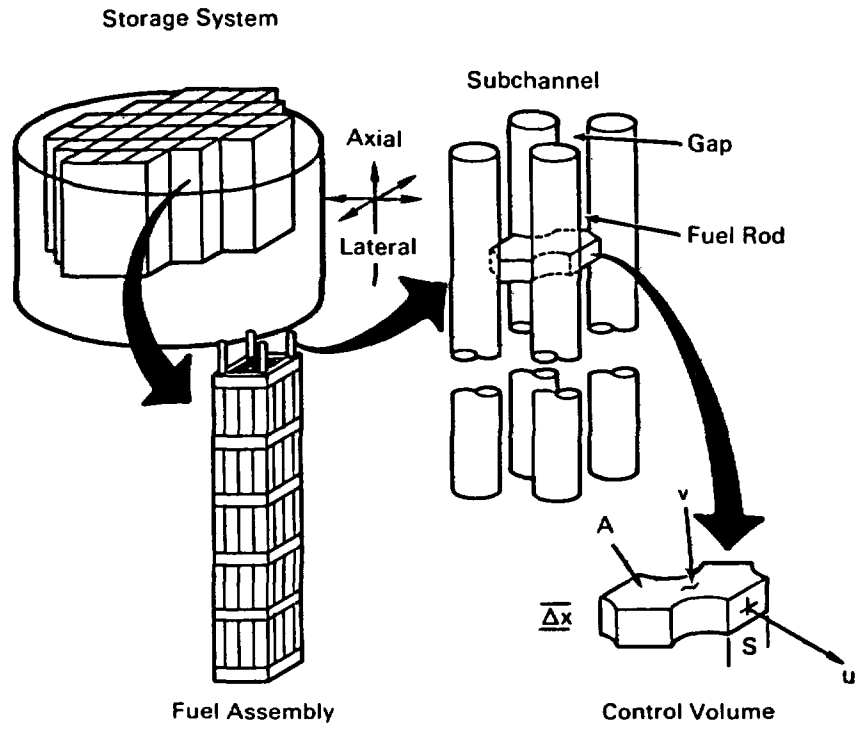

FIGURE 3.1. Relation of Subchannel Control Volume to Storage System

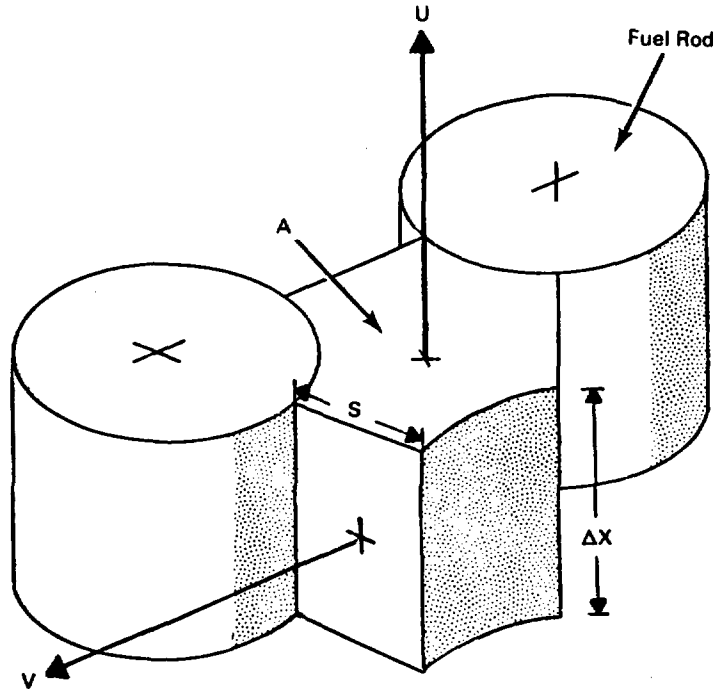

FIGURE 3.2. Subchannel Control Volume

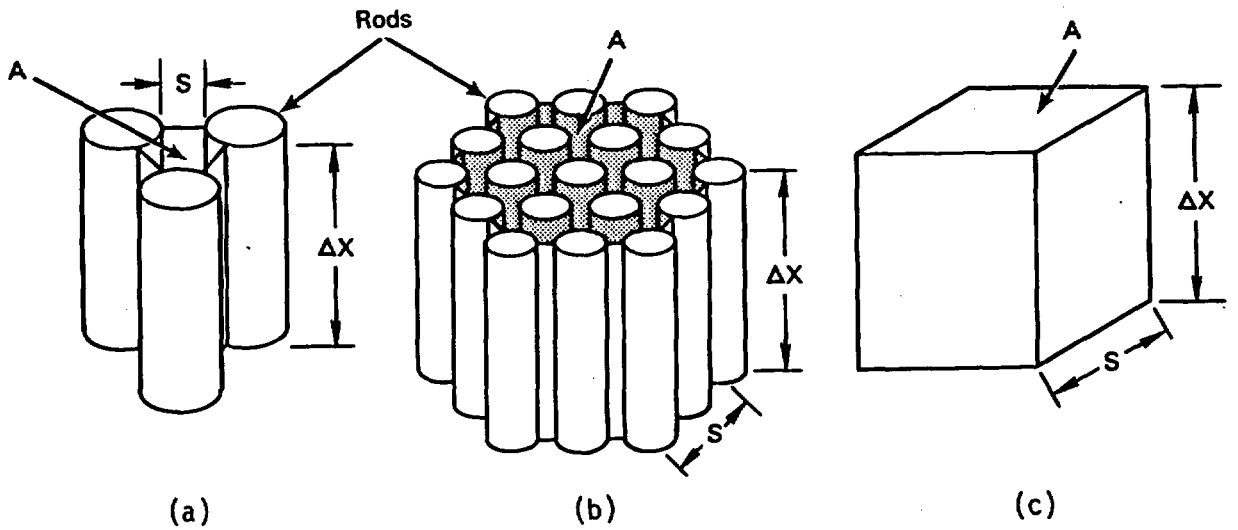

FIGURE 3.3. Possible Control Volume Shapes Using the Generalized Subchannel Noding Approach. (a) Standard Subchannel Noding, (b) Lumped Subchannel Noding, and (c) Noding for Fluid Not in a Rod Array

Lateral flow between adjacent subchannel control volumes passes through a region between separated solid surfaces. The width of the gap between surfaces is S and the lateral velocity is V. Each channel can have an arbitrary number of lateral flow connections (three in the case of Figure 3.2) to adjacent channels, and the gap width, S, may vary from connection to connection.

A fundamental assumption of the subchannel formulation is that any lateral flow is directed by the orientation of the gap it flows through and loses its sense of direction after leaving the gap region. This allows channels to be connected arbitrarily since no fixed lateral coordinate is required. This formulation allows a great deal of flexibility in modeling complex flow problems, since the cross-sectional flow area of a channel and its connection to other channels may be arbitrarily defined. Figure 3.3 shows possible control volume shapes for standard subchannel noding, and for a channel representing several subchannels and noding for a fluid channel not in a rod array.

To develop finite-volume equations, the control volume is represented by the computational cell shown in Figure 3.4, and computational variables are located as shown. The state variables of density, ρ, and enthalpy, h, are defined at the cell center and are indexed by the node number. The axial flow rate, m; pressure, P; and axial flow area, A, are located at the cell boundaries and are indexed by the corresponding node and axial level. The crossflow per unit length, w, and gap width, S, are on the transverse cell boundaries midway between the axial levels and are indexed by the gap number and axial level. In the difference equations, the positions of the variables are indicated by the axial node index (j, j+1, j-1, etc.), where j increases as you move up the channel.

The fluid is assumed to be incompressible but thermally expandable; therefore, the fluid properties, such as density, are expressed as functions of local enthalpy and a uniform reference pressure.

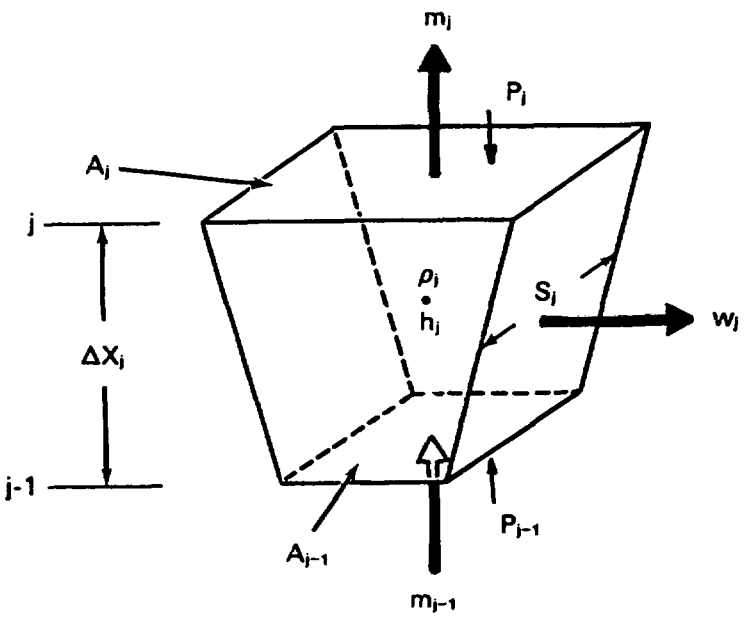

FIGURE 3.4. Subchannel Computational Cell

The conservation equations are formulated using velocity as the transportative variable. However, since COBRA-SFS is derived from previous COBRA versions, the transportation variables are converted to mass flow rate for this code manipulation. The finite difference form of these equations comes directly from the integral statements of the conservation principle for the given control volumes.

3.1.1 Mass Conservation

The control volume used to derive the mass balance equations is given in Figure 3.5. Applying conservation of mass to the reference control volume i, shown in Figure 3.5, gives the following finite-volume equation

$$\bar{A}\Delta x \left(\frac{\rho - \rho^n}{\Delta t}\right) + U_j \rho^* A_j - U_{j-1}\rho^* A_{j-1} + \sum_{k\epsilon\Psi_i} e_{ik}(V_k \rho^* S_k \Delta x)_j = 0 \qquad (3.1)$$

$$\begin{bmatrix}\text{rate of}\\ \text{mass storage}\end{bmatrix} + \begin{bmatrix}\text{mass}\\ \text{transported axially}\end{bmatrix} + \begin{bmatrix}\text{mass transported}\\ \text{laterally}\end{bmatrix} = 0$$

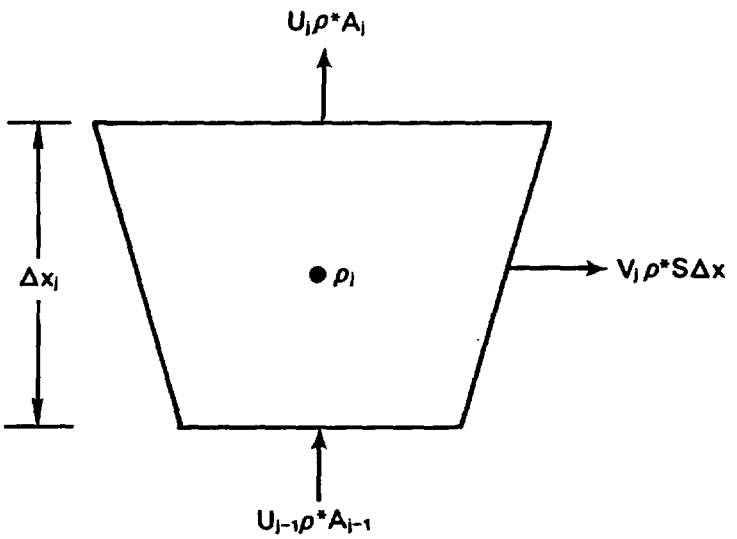

FIGURE 3.5. Mass Balance on a Subchannel Control Volume

where ρ^n is the density at the previous time step and Δt is the time step. The summation of crossflows is performed for all connections, k, that are members of the set, Ψ_i, of all transverse connections to subchannel i. Each lateral flow connection may have a different gap width and flow rate. Here and in the following equations the channel subscript i has been omitted where the reference is clear.

The assumptions made in the derivation of the continuity equation are that the channel area changes linearly with distance over the length of the control volume; the fluid density is uniform throughout the control volume; the axial and lateral velocities are uniform over the respective areas, and the lateral connection width is constant over the length of the control volume.

The axial velocity U is defined as positive in the upward direction (i.e., toward increasing values of j). The transverse velocity V is directed by its gap k such that positive is by definition an outflow from one channel and an inflow to the other. The convection used to determine the direction is that a positive velocity is defined to be from channel ii to channel jj, where ii is the smaller index of two connected channels. To keep track of the sign of the transverse velocity, the switch function, e_{ik}, is used where

$$e_{ik} = \begin{cases} 1 \text{ if the channel index, i, is equal to ii} \\ -1 \text{ if the channel index, i, is equal to jj} \end{cases}$$

Therefore, $e_{ik} = 1$ indicates that positive flow is out of channel i and $e_{ik} = -1$ indicates that positive flow is into channel i. The donor cell convention is used for the convected quantities as indicated by the asterisk. That is

$$\rho^* U_j = \begin{matrix} \rho_j \ U_j & \text{if } U_j \geq 0 \\ \rho_{j+1} \ U_j & \text{if } U_j < 0 \end{matrix} \qquad (3.2)$$

Likewise,

$$\rho^* V_k = \begin{cases} \rho_{ii} V_k & \text{if} \quad V_k \geq 0 \\ \rho_{jj} V_k & \text{if} \quad V_k < 0 \end{cases} \tag{3.3}$$

The axial flow rate is defined to be

$$m_j = \rho^* U_j A_j \tag{3.4}$$

and the transverse flow rate per unit length to be

$$w_k = \rho^* V_k S_k \tag{3.5}$$

The final form of the conservation used in the COBRA-SFS code is

$$\bar{A}_j \frac{\Delta x_j}{\Delta t} (\rho - \rho^n)_j + m_j - m_{j-1} + \Delta x_j \sum_{k \epsilon \Psi_i} e_{ik} w_k = 0 \tag{3.6}$$

3.1.2 Axial Momentum Conservation

In deriving the axial momentum equation, it is assumed that all irreversible losses can be calculated using suitable friction factors and local loss coefficients applied to the bulk velocity. Also, it is assumed that pressure changes linearly along the control volume and that the shear stress on the fluid from adjacent channels can be neglected. It is further assumed that a turbulent cross flow exists between adjacent channels that produces no net mass exchange but does transport momentum laterally at a rate proportional to that of lateral turbulent energy transport.

Applying conservation of momentum to the control volume shown in Figure 3.6 gives the following finite-volume form of the axial momentum equation

$$\Delta x A \left(\frac{\rho U - (\rho U)^n}{\Delta t}\right)_j + \left(\rho^* U_j\right)^* \bar{A}_j \bar{U}_j - \left(\rho^* U_{j-1}\right)^* \bar{A}_j \bar{U}_{j-1} +$$

$$\left[\begin{array}{l}\text{axial momentum}\\ \text{storage}\end{array}\right] + \left[\begin{array}{l}\text{axial momentum}\\ \text{transported axially}\end{array}\right] +$$

$$\sum_{k \epsilon \Psi_i} e_{ik} (\rho^* U)^*_k \bar{V}_k S_k \Delta x + F_T$$

$$\left[\begin{array}{l}\text{axial momentum}\\ \text{transported laterally}\end{array}\right] + \left[\begin{array}{l}\text{turbulent momentum}\\ \text{exchange}\end{array}\right]$$

$$P_{j-1} A_{j-1} - P_j A_j - \bar{P} (A_{j-1} - A_j) + F_s - F_g \qquad (3.7)$$

[pressure forces] - [wall drag forces] - [body forces]

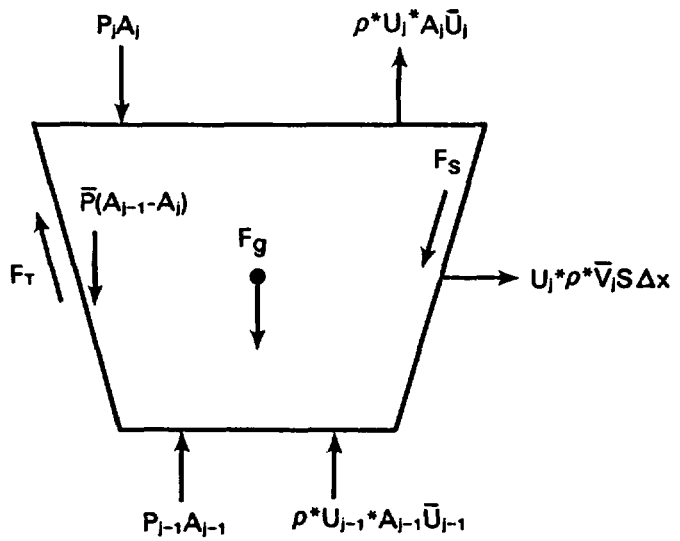

FIGURE 3.6. Axial Momentum Balance on a Subchannel Control Volume

By assuming linear pressure variation and defining

$$\bar{P} = \frac{P_j + P_{j-1}}{2} \tag{3.8}$$

then the pressure difference is written as

$$P_{j-1}A_{j-1} - P_jA_j = \bar{P}\,(A_{j-1} - A_j) + \bar{A}\,(P_{j-1} - P_j) \tag{3.9}$$

Therefore, the pressure force resulting from the area change is cancelled, and

$$P_{j-1}A_{j-1} - P_jA_j - \bar{P}\,(A_{j-1} - A_j) = \bar{A}\,(P_{j-1} - P_j) \tag{3.10}$$

The shear forces exerted by the walls are expressed in terms of empirical wall friction factor correlations and local form loss coefficients. This term is expressed as

$$F_s = \frac{1}{2}\left(\frac{f\Delta x}{D_h} + K\right)\rho U|U|A \tag{3.11}$$

where D_h is the hydraulic diameter, f is the Darcy-Weisbach friction factor and K is the additional form loss coefficient to account for local obstructions such as grid spacers.

The only body force considered is the gravity force. This term is expressed as

$$F_g = \bar{A}\Delta x\ \rho\ g\ \cos\theta \tag{3.12}$$

where θ is the orientation angle of the control volume. For $\theta = 0°$, positive gravity acts downward and opposes positive flow. If $\theta = 90°$, the axial flow is horizontal and gravity has no effect on axial momentum.

In the axial convection of axial momentum, the convected term is combined with the flow area and defined as

$$m_j^* = (\rho^* U_j)^* A \tag{3.13}$$

and

$$\bar{U}_j m_j^* = \begin{cases} \bar{U}_j m_j & \text{if } \bar{U}_j \geq 0 \\ \bar{U}_j m_{j+1} & \text{if } \bar{U}_j < 0 \end{cases}$$

and the transporting velocity, $\bar{U}_j$, is defined as

$$\bar{U}_j = \frac{0.5}{\bar{A}_{j+1}} \left(\frac{m_j}{\bar{\rho}_j} + \frac{m_{j+1}}{\bar{\rho}_{j+1}} \right) \tag{3.14}$$

where

$$\rho_j = 1/2 \quad (\rho_j + \rho_{j+1})$$

For the term defining lateral transport of axial momentum, the convected quantity $(\rho_j^* U_j)^*$ is converted to axial flow rate by multiplying and dividing this term by A_j or

$$(\rho^* U_j)^* = \left(\frac{m_j}{A_j} \right)_k^* \tag{3.15}$$

and

$$\bar{V}_k \left(\frac{m_j}{A_j}\right)^*_k = \begin{cases} \bar{V}_k \frac{m_{ii}}{A_{ii}} & \text{if } \bar{V}_k \geq 0 \\ V_k \frac{m_{jj}}{A_{jj}} & \text{if } \bar{V}_k < 0 \end{cases}$$

The transporting velocity $\bar{V}_k$ is defined as

$$\bar{V}_k = \frac{0.5}{S_k}\left(\frac{w_{k,j}}{\bar{\rho}_{k,j}} + \frac{w_{k,j+1}}{\bar{\rho}_{k,j+1}}\right) \tag{3.16}$$

where

$$\bar{\rho}_k = 1/2\ (\rho_{ii} + \rho_{jj})_k$$

The turbulent momentum exchange, F_T, is modeled using a turbulent crossflow per unit axial length, w_T, as

$$F_T = \sum_{k\epsilon\Psi_i} e_{ik}\, w_T \left(\frac{m_{ii}}{\bar{\rho}_{ii}A_{ii}} - \frac{m_{jj}}{\bar{\rho}_{jj}A_{jj}}\right) f_c \Delta x \tag{3.17}$$

The turbulent crossflow produces no net mass exchange between adjacent channels; however it does transport both momentum and energy from one channel to another. The constant of proportion relating turbulent momentum to turbulent energy transport is f_c. The variable f_c has the same function as a turbulent Prandtl number. If $f_c = 1.0$, energy and momentum are exchanged at equal rates. If $f_c = 0.0$, there is no lateral momentum exchange due to turbulence.

When the above definitions are substituted into equation (3.1-7) the final form is

$$\frac{\Delta x(m_j - m_j^n)}{\Delta t} + m_j^* \bar{U}_j - m_{j-1}^* \bar{U}_{j-1} + \sum_{k\epsilon\Psi_i} \left[e_{ik} \left(\frac{\bar{m}}{\bar{A}}\right)_k^* \bar{V}_k S_k \right]_j \Delta x$$

$$+ \sum_{k\epsilon\Psi_i} e_{ik} W_{T_k} \left(\frac{m_{ii}}{\bar{\rho}_{ii} A_{ii}} - \frac{m_{jj}}{\bar{\rho}_{jj} A_{jj}} \right) f_c \Delta x = \bar{A}_j \left(P_{j-1} - P_j\right) - \frac{1}{2} \left(\frac{f}{D_h} + \frac{K}{\Delta x_j} \right) \left| \frac{m_j}{\rho A} \right| m_j$$

$$- \bar{A} \Delta x \, \rho \, g \cos \theta \qquad (3.18)$$

3.1.3 Transverse Momentum Conservation

A transverse momentum control volume for a standard subchannel noding is shown in Figure 3.7. The gap width between rods is denoted by S and the control volume length is denoted by ℓ. Due to the predominantly axial nature of the flow in rod assemblies, the fluid field solution is relatively insensitive to the dimensions of the transverse momentum control volume. It is assumed that the transverse velocity is normal to the transverse gap inside the control volume.

In deriving the transverse momentum equation, it is assumed that all irreversible losses can be calculated by the use of a single loss coefficient applied to the transverse velocity. Also, it is assumed that transverse momentum is not convected in the transverse direction so that each transverse momentum control volume is independent of the others.

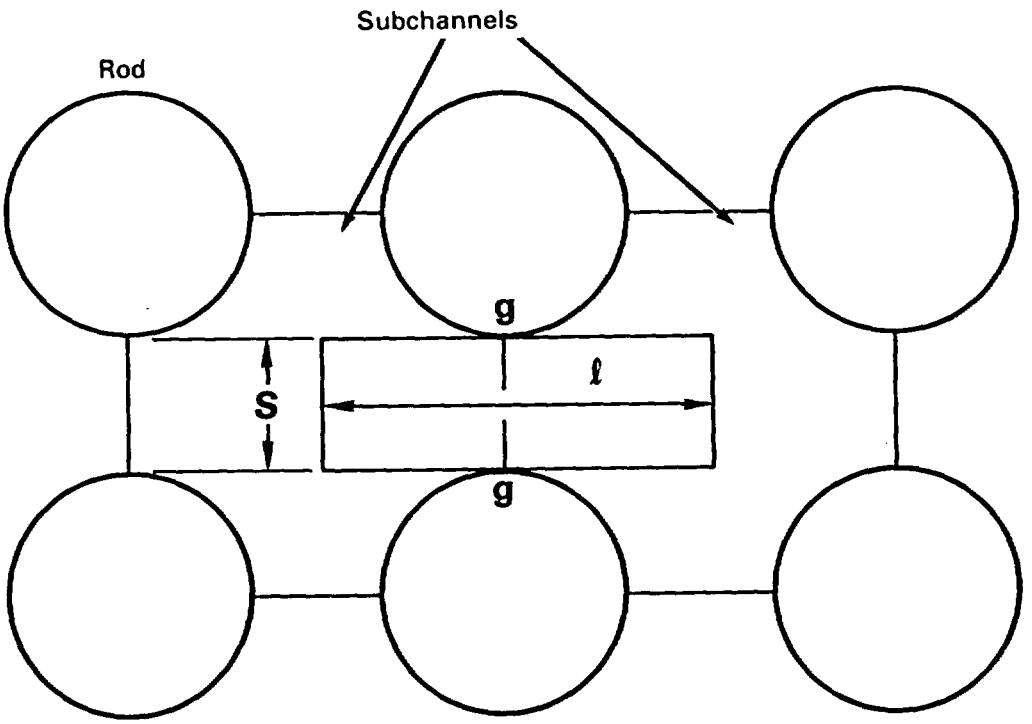

FIGURE 3.7. Transverse Momentum Control Volume

Applying conservation of momentum to the control volume shown in Figure 3.8 gives the following finite-volume form of the transverse momentum equation

$$\Delta x S_k \left(\frac{\rho V - (\rho V)^n}{\Delta t}\right)_j + \rho^* V_j^* S_k \bar{u}_j - \rho^* V_{j-1}^* S_k \bar{u}_{j-1}$$

$$\left[\begin{array}{l}\text{transverse momentum}\\ \text{storage}\end{array}\right] + \left[\begin{array}{l}\text{transverse momentum}\\ \text{transported axially}\end{array}\right]$$

$$= \frac{\Delta x S_k}{\ell_k} g_c (P_{ii} - P_{jj})_{j-1} - F_s \qquad (3.19)$$

$$= \text{[pressure forces]} - \text{[wall shear forces]}$$

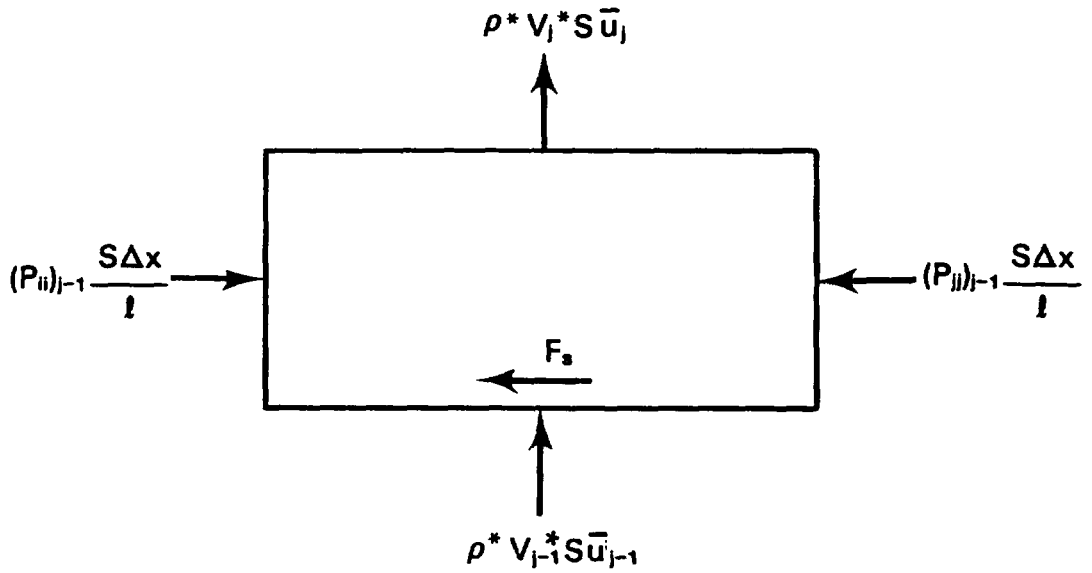

FIGURE 3.8. Transverse Momentum Balance on a Control Volume

The shear forces exerted by the walls and fuel rods are expressed in terms of empirical local form loss coefficients. The shear force per unit length, F_s, is expressed as

$$F_s = -1/2\ K_G|V|V\ \frac{\Delta x S \rho}{\ell} \tag{3.20}$$

where K is the form loss coefficient.

In the axial convection of transverse momentum,

$$w_j^* = \rho^* V_j^* S_k \tag{3.21}$$

the crossflow is used as the convected quantity and the transport terms are expressed as

$$\bar{u}_j \, w_j^* = \begin{cases} \bar{u}_j \, w_j & \text{if } \bar{u}_j \geq 0 \\ \bar{u}_j \, w_{j+1} & \text{if } \bar{u}_j < 0 \end{cases}$$

and the transporting velocity, $\bar{U}_j$, is defined as

$$\bar{u}_j = \frac{1}{(A_{ii}+A_{jj})} \left(\frac{m_{ii}}{\bar{\rho}_{ii}} + \frac{m_{jj}}{\bar{\rho}_{jj}} \right) \tag{3.22}$$

When the above definitions are substituted into Equation (3.19), the finite-volume form used is

$$\Delta x \left(\frac{w_j - w_j^n}{\Delta t} \right) + w_j^* \bar{u}_j - w_{j-1}^* \bar{u}_{j-1} = \frac{S \Delta x g_c}{\ell} (P_{ii} - P_{jj})_{j-1}$$

$$- 1/2 \, K_G \left| \frac{w_j}{\rho S} \right| w_j \frac{\Delta x}{\ell} \tag{3.23}$$

3.2 FLOW SOLUTION METHOD

The finite-volume equations presented in Section 3.1 are written for each fluid node or gap connection in the problem. The RECIRC solution method, adapted from the COBRA-WC code (George et al. 1980), is used to iteratively solve the set of equations to obtain the flow and pressure field. The primary advantage of the RECIRC method is that it is applicable to reverse and recirculating flows, such as those occurring in natural circulation cooled storage systems. RECIRC uses a Newton-Raphson technique similar to the one developed by Hirt (1972) to solve the conservation equations, but it has been made implicit in time as was done in the SABRE code (Gosman et al. 1973). Since the solution method is quite complex, it is summarized below before examining each separate step of the solution method in more detail.

The RECIRC flow field solution routine is divided into two parts: a tentative flow solution and a pressure solution. The tentative flow solution

is achieved by iteratively sweeping the bundle from inlet to exit. In each sweep, the bundle, tentative axial flows, $\tilde{m}$, and crossflow, $\tilde{w}$, are computed by evaluating the two linearized momentum equations with current values for pressures and other variables. (The specific forms of the momentum equations will be described in the following pages.) Then, after all tentative flows and crossflows have been computed at all axial levels, the flows and pressures are adjusted to satisfy continuity by a Newton-Raphson method. The resulting flow field from this pressure solution is then used in the energy equation to obtain an enthalpy and fluid properties distribution for the next axial sweep. A flow chart of this method is shown in Figure 3.9. The tentative flow solution is described in more detail in Section 3.2.1 and the pressure solution is described in Section 3.2.2. The energy solution will be discussed in Section 4.2.

3.2.1 Tentative Flow Solution

The first step is the solution of the axial and transverse momentum equations for the tentative flow rates $\tilde{m}$ and $\tilde{w}$. Since the axial flow in channel i is affected by axial flows in adjacent channels through the crossflow terms, the tentative flows, $\tilde{m}_j$, in all channels at an axial level must be solved for simultaneously. The axial momentum equations are linearized to form a system of N equations, where N is the number of channels.

$$[A]\,\tilde{m}_j = -\,g_c A_j\,(\tilde{P}_j - \tilde{P}_{j-1}) + B \tag{3.24}$$

The diagonal elements of [A] are defined by

$$A_{ii} = \frac{\Delta x}{\Delta t} + \delta_j \bar{U}'_j - \delta_{j-1}\bar{U}_{j-1} + \sum_{k\epsilon\psi_i} \delta_k e_{ik} \bar{V}_k \frac{S_k}{A_i}\,\Delta x + \left(\frac{f}{D_h} + \frac{K}{\Delta x}\right)\left|\frac{m_j}{\rho A}\right|$$

$$+ \sum_{k\epsilon\psi_i} \frac{w_T}{\rho A}\,\Delta x \tag{3.25}$$

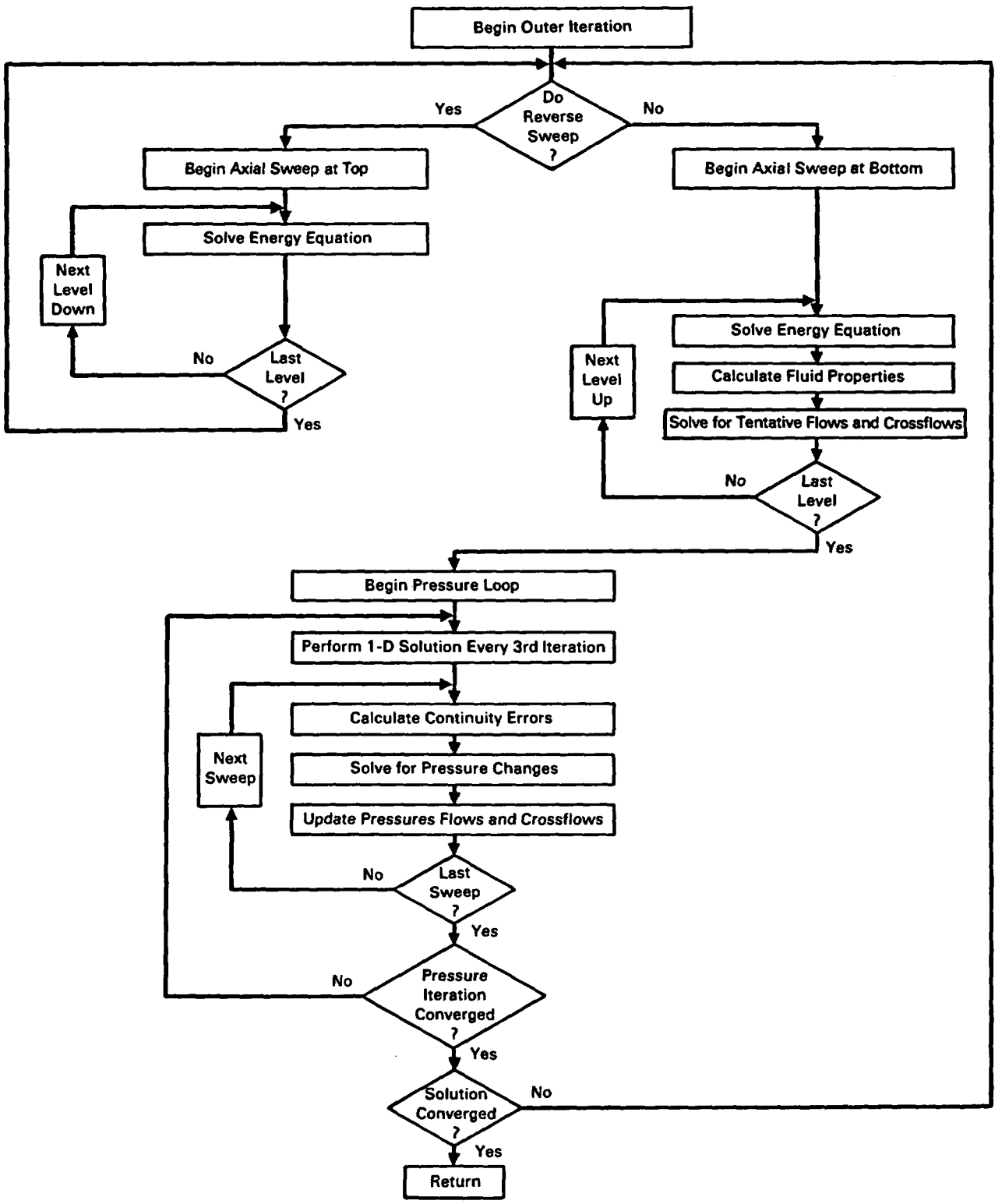

FIGURE 3.9. Flow Chart of the RECIRC Flow Solution Scheme

where the switch function, δ, is defined as

$$\delta_j = \begin{cases} 0 \text{ if } \bar{U}_j \leq 0 \\ 1 \text{ if } \bar{U}_j > 0 \end{cases}$$

$$\delta_{j-1} = \begin{cases} 0 \text{ if } \bar{U}_{j-1} > 0 \\ 1 \text{ if } \bar{U}_{j-1} < 0 \end{cases}$$

$$\delta_k = \begin{cases} 0 \text{ if } e_{ik}\bar{V}_k \leq 0 \\ 1 \text{ if } e_{ik}\bar{V}_k > 0 \end{cases}$$

The off diagonal elements of [A] contain zeros except for the columns representing channels adjacent to channel i where the elements are defined as

$$A_{in} = (1-\delta_k)\, e_{ik}\, \bar{V}_k \left(\frac{S_k \Delta x}{A_n} - \frac{w_T}{\rho_n A_n} \Delta x \right) \tag{3.26}$$

where n = II+JJ-i

In the above definition, the subscript n refers to a channel adjacent to i. II and JJ represent the channels connected by gap k.

The constant B is the source terms calculated as

$$B_i = \bar{A}\Delta x \rho g \cos\theta + \frac{1}{2}\left(\frac{f}{D_h} + \frac{K}{\Delta x_j}\right)\left|\frac{m_j}{\rho A}\right| m_j - (1-\delta_j)\, m_{j+1}\, \bar{U}_j$$

$$+ (1-\delta_{j-1})\, m_{j-1}\, \bar{U}_{j-1} + \frac{\Delta x}{\Delta t} m_j^n \tag{3.27}$$

The pressures and flow rates in Equation (3.27) are those generated during the previous pressure iteration, except m_{j-1}, which is a predicted axial flow rate discussed later in this section. To insure that friction effects have the proper weight when diferentiating Equation (3.24) with respect to pressure, the linearized pressure loss is defined as

$$\Delta P_f = -1/2 \left(\frac{f}{D_h} + \frac{K}{\Delta x}\right) \left|\frac{m_j}{\rho A}\right| (2\tilde{m}_j - m_j) \tag{3.28}$$

Equation (3.24) is compacted to a matrix containing only nonzero terms and solved by direct elimination at each level.

Once a set of tentative axial flows, $\tilde{m}$, has been obtained, the tentative crossflows, $\tilde{w}$, are calculated. Since the transverse momentum equation does not depend on crossflows in other gaps, a simultaneous solution is not necessary, and the tentative crossflows in each gap are calculated using the linearized form of Equation (3.23)

$$\tilde{w}_j = \left[\frac{S\Delta gc}{\ell} (P_{ii}-P_{jj})_{j-1} - (1-\delta_j)\, w_{j+1}\bar{u}_j + (1-\delta_{j-1})\, w_{j-1}\bar{u}'_{j-1} + \frac{\Delta x}{\Delta t}\, w_j^n \right.$$
$$\left. + 1/2\, K_G \left|\frac{w_j}{\rho S}\right| w_j \frac{\Delta x}{\ell}\right] \Bigg/ \left[\frac{\Delta x}{\Delta t} + \delta_j \bar{u}_j - \delta_{j-1}\bar{u}'_{j-1} + K_G \left|\frac{w_j}{\rho S}\right| \frac{\Delta x}{\ell}\right] \tag{3.29}$$

The pressures and flow rates used in Equation (3.29) are those generated during the previous pressure iteration, except for $\bar{u}'_{j-1}$, a velocity based on the predicted axial flow rate m'_{j-1}. The tentative flow field is determined for each channel and gap for the complete problem domain by sweeping the assemble from inlet to exit. Note that at this stage the tentative flows and crossflows do not, in general, satisfy continuity.

The efficiency of the overall solution can be enhanced if the flow rate used to define the donor cell axial momentum flux is forced to satisfy continuity during the tentative flow axial sweep. This is accomplished by defining a set of "predicted" axial flows m_j at level j that are used to

evaluate the tentative flow rate at level j+1. The predicted flows are determined by solving the combined linearized momentum and continuity equations while assuming that the previous axial level flows are fixed. At level j only, the continuity error for each cell is calculated as

$$E_j = \bar{A}_j \ \Delta x_j/\Delta t \ (\rho - \rho^n)_j + \tilde{m}_j - m'_{j-1} + \Delta x_j \sum_{k\epsilon\Psi_i} e_{ik} \ w'_{j-1} \qquad (3.30)$$

where m'_{j-1} and w'_{j-1} are predicted flows calculated at the previous axial level and $\tilde{m}_j$ is the just-computed tentative axial flow. Estimated pressure changes, $\delta P'_j$, are calculated from the Newton-Raphson expression

$$\delta P'_{j-1} \frac{\partial \tilde{m}_j}{\partial P_{j-1}} + \sum_{k\epsilon\Psi_i} \delta P'_{n,j-1} \frac{\partial \tilde{w}_j}{\partial P_{n,j-1}} = - E_j \qquad (3.31)$$

where n = ii+jj-i and the pressure derivatives are the same as those defined later in the pressure solution section.

Once a set of estimated pressure changes are calculated, the predicted flows to be used in the donor momentum flux terms for the next axial level are calculated using

$$m'_j = \tilde{m}_j + \frac{\partial \tilde{m}_j}{\partial P_{j-1}} \delta P'_{j-1} \qquad (3.32)$$

$$w'_j = \tilde{w}_{j-1} + \frac{\partial \tilde{w}_j}{\partial P_{j-1}} \ (\delta P'_{ii,j-1} - \delta P'_{jj,j-1}) \qquad (3.33)$$

The tentative flows and pressures are not updated using this information. The predicted flows are used only to provide a better estimate of the donor momentum flux distribution to the momentum equations at the next axial level.

The predicted average axial velocity in the gap, used in Equation (3.29), is calculated as

$$\bar{u}'_j = \left(\frac{m'_{ii}}{\bar{\rho}_{ii}} + \frac{m'_{jj}}{\bar{\rho}_{jj}} \right) (A_{ii} + A_{jj})^{-1} \tag{3.34}$$

For forced convection problems, the convergence is substantially improved if the predicted value for the axial momentum flux is used. For problems with negative flows or buoyancy-dominated flows, the use of predicted momentum flux can be counterproductive. The calculation of a predicted momentum flux is automatically skipped if negative flows occur in an assembly.

3.2.2 Pressure And Linearized Flow Solution

After all tentative axial flows and crossflows have been computed at all axial levels in all assemblies, the pressures and flows are adjusted to satisfy continuity. The flow and pressure field in each assembly are locally independent of all the other assemblies for a given boundary condition. Therefore, the equations for flow and pressure are solved on an assembly-by-assembly basis. The first step in this process is to compute the continuity error, E_j, in all cells using the expression

$$E_j = \bar{A}_j \, \Delta x_j / \Delta t \, (\rho - \rho^n)_j + \tilde{m}_j - \tilde{m}_{j-1} + \Delta x_j \sum_{k \epsilon \Psi_i} e_{ik} \tilde{w}_j \tag{3.35}$$

The adjustments in axial flows and crossflows necessary to satisfy continuity are defined as

$$\Delta m_j = m_j - \tilde{m}_j \tag{3.36a}$$

$$\Delta w_j = w_j - \tilde{w}_j \tag{3.36b}$$

$$\Delta m_{j-1} = m_{j-1} - \tilde{m}_{j-1} \tag{3.36c}$$

where m and w are flows that satisfy continuity.

By substituting these expressions into Equation (3.35) and subtracting Equation (3.6), the flow adjustments must satisfy the expression

$$\Delta m_j - \Delta m_{j-1} + \Delta x_j \sum_{k \epsilon \psi_i} e_{ik} \Delta w_j = - E_j \tag{3.37}$$

Assuming that m and w are functions of pressure only, the flow corrections can be expressed as

$$\Delta m_j = \frac{\partial \tilde{m}_j}{\partial P_{j-1}} \delta P_{j-1} + \frac{\partial \tilde{m}_j}{\partial P_j} \delta P_j \tag{3.38a}$$

$$\Delta w_j = \frac{\partial \tilde{w}_j}{\partial P_{j-1}} \delta P_{i,j-1} + \frac{\partial \tilde{w}_j}{\partial P_{n,j-1}} \delta P_{n,j-1} \tag{3.38b}$$

$$\Delta m_{j-1} = \frac{\partial \tilde{m}_{j-1}}{\partial P_{j-1}} \delta P_{j-1} + \frac{\partial \tilde{m}_{j-1}}{\partial P_{j-2}} \delta P_{j-2} \tag{3.38c}$$

where n is the channel adjacent to channel i. The expressions for the flow and crossflow derivatives are derived from the linearized form of the axial and transverse momentum equations [Equations (3.24) and (3.29)] and are presented in Table 3.1.

TABLE 3.1. Flow Derivatives with Respect to Pressure

Flow Derivative	Definition[(a)]
$\frac{\partial \tilde{m}_j}{\partial P_{j-1}} = - \frac{\partial \tilde{m}_j}{\partial P_j}$	$\frac{gc\bar{A}_j}{A_{ii}}$
$\frac{\partial \tilde{w}_j}{\partial P_{ii,j-1}} = - \frac{\partial \tilde{w}_j}{\partial P_{jj,j-1}}$	$\frac{S}{\ell} \frac{\Delta x gc}{C_j}$

(a) A_{ii} is defined in Equation (3.25).
C_j is the denominator Equation (3.29).

After substituting in these expressions for flow correction and rearranging, Equation (3.36) takes the general form

$$-\frac{\partial \tilde{m}_{j-1}}{\partial P_{j-2}}\,\delta P_{j-2}+\left[\frac{\partial \tilde{m}_j}{\partial P_{j-1}}-\frac{\partial \tilde{m}_{j-1}}{\partial P_{j-1}}+\Delta x_j\sum_{k\epsilon\Psi_i} e_{ik}\frac{\partial \tilde{w}_j}{\partial P_{i,j-1}}\right]\delta P_{j-1}$$

$$+\frac{\partial \tilde{m}_j}{\partial P_j}\,\delta P_j+\Delta x\sum_{k\epsilon\Psi_i} e_{ik}\frac{\partial \tilde{w}_j}{\partial P_{n,j-1}}\,\delta P_{n,j-1}=-E_j \qquad (3.39)$$

which is equivalent to

$$\frac{\partial E_j}{\partial P_{j-2}}\,\delta P_{j-2}+\frac{\partial E_j}{\partial P_{j-1}}\,\delta P_{j-1}+\frac{\partial E_j}{\partial P_j}\,\delta P_j+\sum_{k\epsilon\Psi_i}\frac{\partial E_j}{\partial P_{n,j-1}}\,\delta P_{n,j-1}=-E_j \qquad (3.40)$$

where the $\partial E/\partial P$ terms are given in Table 3.2.

TABLE 3.2. Continuity Error Derivatives with Respect to Pressure

Error Derivative	Definition
$\frac{\partial E_j}{\partial P_{j-1}}$	$\frac{\partial \tilde{m}_j}{\partial P_{j-1}}-\frac{\partial \tilde{m}_{j-1}}{\partial P_{j-1}}+\Delta x_j\sum_{k\epsilon\psi_i} e_{ik}\frac{\partial \tilde{w}_j}{\partial P_{i,j-1}}$
$\frac{\partial E_j}{\partial P_{j-2}}$	$-\frac{\partial \tilde{m}_{j-1}}{\partial P_{j-2}}$
$\frac{\partial E_j}{\partial P_j}$	$\frac{\partial \tilde{m}_j}{\partial P_j}$
$\sum_{k\epsilon\psi_i}\frac{\partial E_j}{\partial P_{n,j-1}}$	$-\Delta x_j\sum_{k\epsilon\psi_i} e_{ik}\frac{\partial \tilde{w}_j}{\partial P_{n,j-1}}$

When the above expression is evaluated for all axial nodes M and all flow channels Q for a given assembly the coefficient matrix consists of N equations, where N is the total number of cells in the assembly (N = M•Q). The matrix equation has the form

$$\begin{bmatrix} \partial E_1/\partial P_1 & \cdots & \partial E_1/\partial P_N \\ \vdots & & \\ \partial E_N/\partial P_1 & \cdots & \partial E_N/\partial P_N \end{bmatrix} \begin{Bmatrix} \delta P_1 \\ \vdots \\ \delta P_N \end{Bmatrix} = \begin{Bmatrix} E_1 \\ \vdots \\ E_N \end{Bmatrix} \qquad (3.41)$$

Since it is generally not possible to solve a matrix of this size directly, the matrix is solved in pieces. An alternating direction iterative solution is implemented that performs a level-by-level sweep followed by a channel-by-channel sweep for each iteration in the pressure loop.

First, the pressure change in each channel in the assembly is determined at each axial level using current values of pressure change in adjacent axial levels. The equation for continuity error becomes

$$\frac{\partial E_j}{\partial P_{i,j-1}} \delta P_{i,j-1} + \sum_{k \epsilon \Psi_i} \frac{\partial E_j}{\partial P_{n,j-1}} \delta P_{n,j-1} = - E_j - \frac{\partial E_j}{\partial P_{j-2}} \delta P^o_{j-2} - \frac{\partial E_j}{\partial P_j} \delta P^o_j \qquad (3.42)$$

where δP^o_j and δP^o_{j-2} are the recent values of the pressure change at axial levels above and below the current level, respectively. For all Q channels in the assembly at axial level j, this equation produces a system of Q equations having the form

$$\begin{bmatrix} \frac{\partial E_{1,j}}{\partial P_{1,j-1}} & \cdots & \frac{\partial E_{1,j}}{\partial P_{Q,j-1}} \\ \vdots & & \vdots \\ \frac{\partial E_{Q,j}}{\partial P_{1,j-1}} & \cdots & \frac{\partial E_{Q,j}}{\partial P_{Q,j-1}} \end{bmatrix} \begin{Bmatrix} \delta P_{1,j-1} \\ \vdots \\ \delta P_{Q,j-1} \end{Bmatrix} = \begin{Bmatrix} -E_{1,j} - \frac{\partial E_{1,j}}{\partial P_{j-2}} \delta P^{o}_{j-2} - \frac{\partial E_{1,j}}{\partial P_{j}} \delta P^{o}_{j} \\ \vdots \\ -E_{Q,j} - \frac{\partial E_{Q,j}}{\partial P_{j-2}} \delta P^{o}_{j-2} - \frac{\partial E_{Q,j}}{\partial P_{j}} \delta P^{o}_{j} \end{Bmatrix} \quad (3.43)$$

This matrix is solved by direct inversion to obtain new δP values for the current level j.

On the second pass the pressure changes at all axial levels are found for each channel of the assembly using current values for the pressure changes in adjacent channels. The equation for continuity error is

$$\frac{\partial E_j}{\partial P_{j-2}} \delta P_{j-2} + \frac{\partial E_j}{\partial P_{i,j-1}} \delta P_{i,j-1} + \frac{\partial E_j}{\partial P_j} \delta P_j = -E_j - \sum_{k \epsilon \Psi_i} \frac{\partial E_j}{\partial P_{n,j-1}} \delta P^{o}_{n,j-1} \quad (3.44)$$

where $\delta P^{o}_{n,j-1}$ is the current pressure change in adjacent channel n. Considering all M axial levels, this equation forms a tridiagonal system of M equations for channel i of the form

$$\begin{bmatrix} \frac{\partial E_{1,2}}{\partial P_{1,1}} & \frac{\partial E_{1,2}}{\partial P_{1,2}} & 0 & \cdots & 0 \\ & & & & \\ & & & & \\ & & & & \\ 0 & \cdots & \frac{\partial E_{i,M+1}}{\partial P_{i,M-1}} & \frac{\partial E_{i,M+1}}{\partial P_{i,M}} & \end{bmatrix} \begin{Bmatrix} \delta P_{i,1} \\ \vdots \\ \delta P_{i,M} \end{Bmatrix} = \begin{Bmatrix} -E_{i,2} + \sum_{k \epsilon \Psi_i} \frac{\partial E_{i,2}}{\partial P_{n,1}} \delta P^{o}_{n,1} \\ \vdots \\ -E_{i,M+1} \sum_{k \epsilon \Psi_i} \frac{\partial E_{i,M+1}}{\partial P_{n,M}} \delta P^{o}_{n,M} \end{Bmatrix} \quad (3.45)$$

which is solved to obtain new δP values for the current channel.

The pressure solution is a potentially time-consuming process for large problems. To solve the equation more efficiently, a one-dimensional axial approximation of the problem is solved after a certain number of level-by-

level and channel-by-channel sweeps. To form the one-dimensional tridiagonal matrix equation, the total continuity error at each level is calculated as

$$\bar{E}_j = \sum_{i=1}^{Q} E_{ij} \tag{3.46}$$

A tridiagonal matrix is then formed:

$$[G]\ \{\overline{\delta P}\} = \bar{E} \tag{3.47}$$

where $G_{ij} = \partial \bar{E} / \partial \overline{P_j}$

which is solved to obtain an average pressure correction, $\overline{\delta P}_j$, at each level, which is then applied to the pressures at that level.

During the pressure loop, the computational mesh is repeatedly swept, level-by-level and channel-by-channel, solving for δP, until the change in all of the δP values falls below a specified convergence criteria.

After the solution to the pressure equation has converged, the resulting pressure changes, δP values, represent adjustments to the pressure field that make the flow field satisfy continuity. The pressures and flows are then updated using

$$P_{i,j} = P^{o}_{i,j} + \delta P_{i,j} \tag{3.48}$$

$$m_j = \tilde{m}_j + \frac{\partial \tilde{m}_j}{\partial P_{i,j-1}} (\delta P_{i,j-1} - \delta P_{i,j}) \tag{3.49}$$

$$w_j = \tilde{w}_j + \frac{\partial \tilde{w}_j}{\partial P_{i,j-1}} (\delta P_{ii,j-1} - \delta P_{jj,j-1}) \tag{3.50}$$

where $P^{o}_{i,j}$ is the pressure from the previous outer iteration. The flow solution now satisfies both momentum and continuity for the current set of properties and boundary conditions. The method is then repeated for each assembly in the problem domain. The new flow field is used in the energy solution to determine the amount of convection heat transfer occurring within the problem. The energy solution is described in more detail in Section 4.2.

3.3 CONSTITUTIVE FLOW MODELS

To close the system of equations described in the previous sections, a set of constitutive relationships is required. For example, the friction factor and form loss coefficients serve to close the momentum equation solution. The constitutive models presented below are empirical in nature and, therefore, should be applied with care since they may be valid only over a certain range of conditions.

3.3.1 Friction Factor Correlations

The shear stress term in the axial momentum equation is expressed in the form

$$F_s = 1/2 \left(\frac{f\Delta x}{D_h} + K \right) \frac{|m|m}{\rho A} \tag{3.11}$$

where f is the Darcy-Weisback friction factor and K is the form loss coefficient. The friction factor for turbulent flow is obtained from the expression

$$f = aRe^{b} + cRe^{d} + e \tag{3.51}$$

where Re is the subchannel Reynolds number, defined as

$$Re = \frac{mD_h}{A\mu} \tag{3.52}$$

and a, b, c, d, and e are specified constants.

Several friction factor correlations may be input and applied to different subchannels within the problem. A second friction factor correlation may be input for laminar flow conditions, which has the form

$$f = a\ell Re^{B\ell} + C\ell \tag{3.53}$$

where $a\ell$, $B\ell$, and $C\ell$ are specified constants.

When both turbulent and laminar flow correlations are specified, the largest of the two friction factors at a given Reynolds number is used in the axial momentum equation.

The friction factor described above is based on subchannel averaged fluid viscosities. As an input option, the friction factor may be corrected for the viscosity variation near a heated surface by using the relationship (Tong 1968)

$$\frac{f_{corr}}{f} = 1 + \frac{P_H}{P_w}\left[\left(\frac{\mu_{wall}}{\mu_{bulk}}\right)^{0.6} - 1\right] \tag{3.54}$$

where f_{corr} is the corrected friction factor, f is the friction factor using bulk fluid properties, P_H is the heated perimeter, P_w is the wetted perimeter and μ_{wall} is the viscosity evaluated at the wall temperature. The wall temperature is calculated from

$$T_{wall} = T_{bulk} + \frac{q'}{P_h H} \tag{3.55}$$

where H is the channel heat transfer coefficient. This correction is based on the assumption that the total perimeter of the channel consists of two regions: one heated (P_h) with a uniform flux (designated q') and the other unheated ($P_w - P_h$).

3.3.2 Form Loss Coefficients

Loss coefficients are used to represent additional pressure losses across grid spacers, orifice plates, and other local flow obstructions in the axial direction. The pressure drop across an obstruction is expressed as

$$\Delta P = \frac{k|m|m}{2g_c \rho A^2} \tag{3.56}$$

where K is a local loss coefficient.

This formulation can be used to model flow through any sudden contraction or expansion where the change in flow results in irreversible losses that cannot be modeled completely with an area change alone. These loss coefficients are specified as a constant or as a function of Reynold's number in tabular form.

The pressure loss in lateral flow through a gap is treated as a local loss rather than a wall friction loss. This permits the formulation of the pressure loss in terms of the known geometric quantities:

$$\Delta P = \frac{K_G|w|w}{2g_c \rho S^2} \tag{3.57}$$

where K_G is the transverse loss coefficient.

In rod assemblies, the coefficient K_G can be thought of as the form loss for flow through the gap between two adjacent fuel rods. The value for K_G is dependent on the geometry of the given problem and must be specified through input.

An additional option exists to specify complete flow blockages in the axial direction. The blockages are specified by subchannel and axial level.

3.3.3 Turbulent Mixing Correlations

A fluctuating crossflow per unit length, w_T, is computed as a fraction of the average axial flow. The fluctuating crossflow performs an equal mass exchange between adjacent subchannels.

The turbulent mixing correlations give the user a choice of four different forms (Rogers and Todreas 1968; Ingesson and Hedberg 1970; Rogers and Rosehart 1972):

$$1)\quad w_T = \beta S_k G' \tag{3.58}$$

$$2)\quad w_T = a\ Re^b S_k\ G' \tag{3.59}$$

$$3)\quad w_T = a\ Re^b\ D'\ G' \tag{3.60}$$

$$4)\quad w_T = a\ Re^b\ \frac{S_k}{z_k}\ D'\ G' \tag{3.61}$$

where $Re = \frac{G'D'}{\mu}$

$$D' = 4\ (A_{ii} + A_{jj})/(P_{w_{ii}} + P_{w_{jj}})$$

$$G' = (m_{ii} + m_{jj})/(A_{ii} + A_{jj})$$

The user may specify different correlations or different coefficients for each assembly type.

3.4 FLOW BOUNDARY CONDITIONS

To solve the system of equations described in the previous sections, some form of flow boundary condition must be specified. Several types of boundary conditions are available in the COBRA-SFS code. These boundary condition options include the following:

- Option 1 - Specify the inlet axial mass flux. This may be a uniform

axial mass flux for all channels or it may be specified for each assembly and/or subchannel.

- Option 2 - Specify an average axial mass flux, but have the code split the total flow so that a uniform pressure gradient exists at the inlet.
- Option 3 - Specify a total axial pressure drop across the system. The code then determines the inlet axial flow for each channel.
- Option 4 - Specify a total flow and an equal pressure drop across all channels. The code then splits the total flow to give a uniform pressure drop across the system.

In all cases an inlet mass flux must be specified. For the first option, the mass fluxes remain constant. For the second option, a new set of mass fluxes reflecting a uniform inlet pressure gradient are calculated and are then frozen. For the third and fourth options, the specified mass flux distribution is used as an estimate until enough information is available to perform a flow field calculation based on pressure.

The uniform inlet pressure gradient option (option two) is described in more detail in Section 3.4.1. The total pressure drop (option three) is applied to all channels in the problem unless pressure losses must be accounted for in the plenum regions. These losses are modeled using the network model, which is described in Section 3.4.2. The transient forcing functions applied to the flow or pressure boundary conditions are described in Section 3.4.3.

3.4.1 Uniform Inlet Pressure Gradient Option

To split the flow for a uniform inlet pressure gradient, an adjustment is made to the inlet flow, m_i, in each channel, so that its inlet pressure gradient $(DP/DX)_i$, is equal to the average inlet pressure gradient. The pressure gradient is assumed to be proportional to the square of the inlet flow

$$(DP/DX)_i = Cm_i^2 \tag{3.62}$$

The change in pressure gradient due to a change in the inlet flow is found by forming the derivative of Equation (3.62)

$$\Delta(DP/DX)_i = 2Cm_i\Delta m_i \tag{3.63}$$

The flow change, Δm_i, is expressed by solving Equation (3.63) for Δm_i and substituting Equation (3.62) for the constant, C.

$$\Delta m_i = \frac{\Delta(DP/DX)_i}{2(\overline{DP/DX})_i} m_i \tag{3.64}$$

The change in pressure gradient is the difference between the average pressure gradient and that in channel i.

$$\Delta(DP/DX)_i = (\overline{DP/DX}) - (DP/DX)_i \tag{3.65}$$

where

$$(\overline{DP/DX}) = \frac{\sum_{i=1}^{N} A_i(DP/DX)_i}{\sum_{i=1}^{N} A_i}$$

N is the number of channels, A_i is the axial flow area, and $(DP/DX)_i$ is computed from the axial momentum equation.

The inlet flows are adjusted by combining Equations (3.64) and (3.65) to give

$$m_i' = m_i + \Delta m_i = m_i + \frac{1}{2}\left[\frac{(\overline{DP/DX}) - (DP/DX)_i}{(DP/DX)_i}\right] m_i \tag{3.66}$$

Equation (3.66) and the axial momentum equations are repeated in turn until the flow change is sufficiently small. This is done immediately after the inlet flow data is read in, before the main flow solution begins.

To ensure that the total flow is conserved, the adjusted flows are re-normalized each iteration by

$$m_i = m_i' \frac{\sum_{i=1}^{N} m_i^o}{\sum_{i=1}^{N} m_i'} \qquad (3.67)$$

where m_i' is given by Equation (3.66) and m_i^o is the initial input inlet flow.

Even though the COBRA-SFS code has not been validated for transient calculations, the final inlet flow split from a steady-state solution would be used without further adjustment in a transient analysis. However, the total flow may change by the input forcing function on the inlet mass flow. The specified mass flux or total pressure options can be applied in both the steady state and transient. Since the pressure drop is very sensitive to changes in inlet flow, the flow split calculation may not converge in transients for very small time steps or if there are severe changes in the flow field. In such cases, the inlet flow split must be specified directly.

3.4.2 Network Model

The specified total pressure drop boundary condition is generally applied uniformly to all channels. However, for many modeling situations, it may be desirable to allow the code to calculate the flow distribution between assemblies based on the orificing and assembly arrangement. The network model has been developed for the COBRA-SFS code to model the pressure losses above and below the channel region. When the network model is used, a single pressure drop is specified as a function of time, and the subchannel flow rates are adjusted so that the pressure drop through each possible flow path matches the specified pressure drop.

Figure 3.10 is a schematic description of the network model for a three-assembly problem with a bypass channel. The conservation equations described in the previous section are solved only for the channel region as noted in Figure 3.10. This channel region formally represents the rod assembly where flow resistance is given by friction factors and loss coefficients. The gravitational head is also accounted for in this region. Along the rest of the flow paths, a reduced momentum equation is solved, which takes into account only the flow resistance due to friction and form and the gravitational head. No inertia terms are included. It is assumed that the transport time through the network model is zero.

In the example described by Figure 3.10, the resistances marked R_{AIN} and R_{AOUT} would be the flow resistances associated with the assembly inlet orifices and the outlet hardware (handling socket, etc.), respectively. The loss coefficients can be made dependent on Reynolds number. A gravitational pressure drop can also be modeled by supplying head lengths at the inlet and outlet. This is noted as H_A in Figure 3.10. The assembly inlet gravitational head is calculated using the inlet temperature to define the density. The outlet gravitational head is calculated using the mixed mean assembly outlet temperature.

The assembly group dynamic loss coefficients, R_{GIN} and R_{GOUT}, represent the flow resistance from a common plenum to assembly group plenums or to the down corner region. The group dynamic loss coefficients are assumed to be independent of Reynolds number. Here too, gravitational losses may be modeled by supplying head lengths. Finally, R_T may represent the dynamic loss coefficient for flow from the inlet nozzle to the common plenum.

For most problems the actual loss coefficients for each of these resistances will not be known, but the flow and corresponding pressure drop across each resistance should be available. The effective loss coefficients may then be calculated as

$$R = \frac{\Delta P g_c}{m^2} \tag{3.68}$$

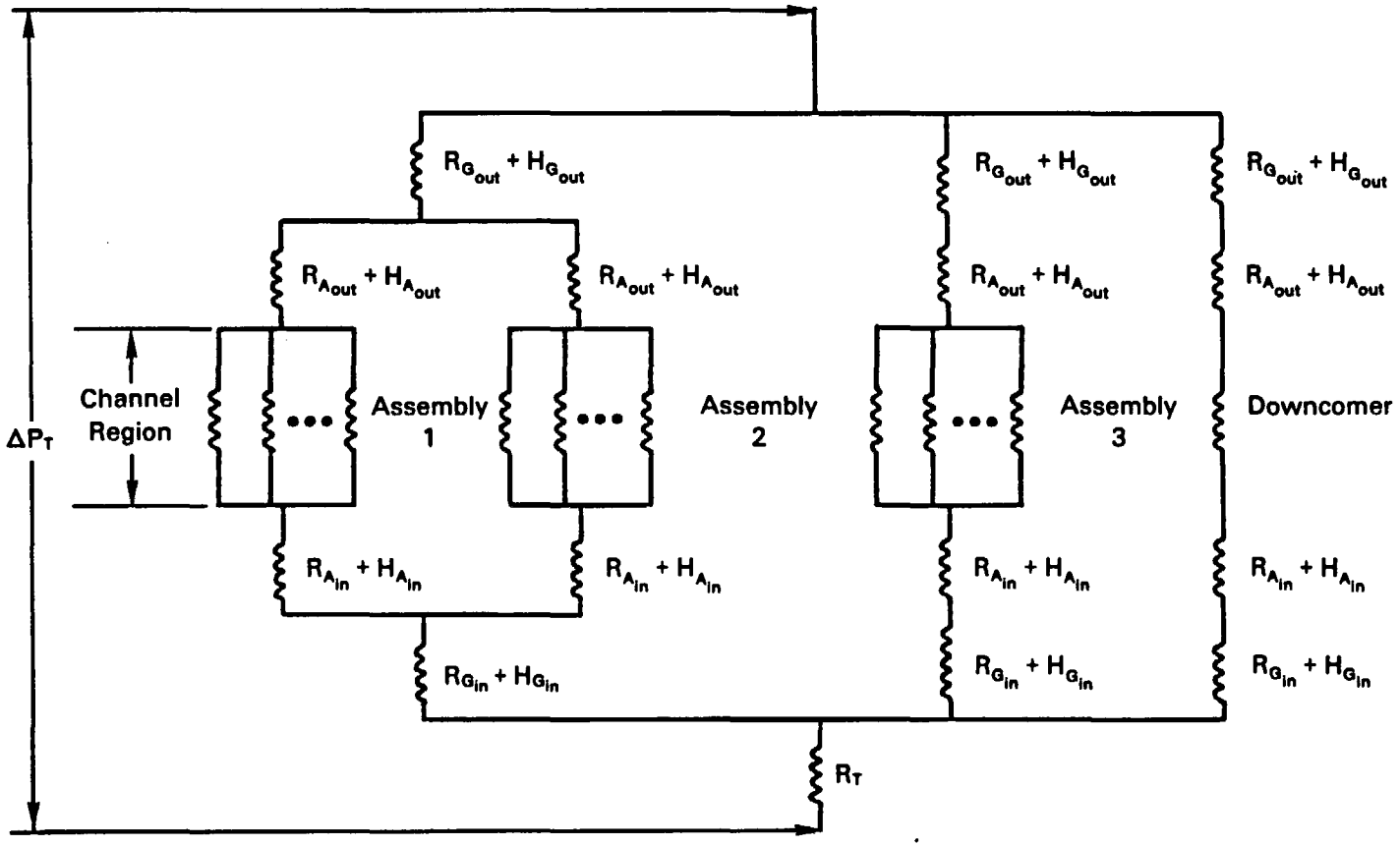

FIGURE 3.10. Schematic Description of the Network Model for Pressure Drop Through Reactor Vessel

For R_A, which may be dependent on Reynolds number, it is necessary to supply a wetted perimeter so the Reynolds number can be calculated from the flow rate. The wetted perimeter need not have any physical significance but should be chosen so that the correct loss is obtained for a given flow rate when using the specified resistance versus Reynolds number curve.

3.4.3 Transient Forcing Functions

Even though the COBRA-SFS code has not been validated for transient calculations, to simulate transients the inlet enthalpy, heat generation, system pressure, and inlet flows can be specified as a function of time. COBRA-SFS reads a table of time versus relative (or actual) value for each parameter to be varied. Linear interpolation is used to obtain values between specified time entries. The value of parameter P at time t is computed as

$$P(t) = F(t)P(o) \tag{3.69}$$

where F(t) is the factor interpolated from the input transient table at time t and P(o) is the steady-state value of parameter P. Alternatively, the actual value of the parameter may be used in the table, so that

$$P(t) = F(t) \tag{3.70}$$

where F(t) is the value interpolated from the table at time t.

The factors entered in the forcing functions tables apply to any of the input options available for that parameter. For example, the inlet enthalpy forcing function table applies to average inlet enthalpy, average inlet temperature, or to individual channel inlet enthalpy or temperature, depending on the input option selected.

Flow forcing functions may be used with any inlet flow option, including the uniform inlet pressure gradient option. Alternatively, a forcing function may be specified for the uniform pressure drop option. If the pressure drop is specified, a flow forcing function becomes the pressure drop forcing function and the inlet flows are computed in response to the pressure boundary condition. The forcing functions do not apply to the total flow boundary condition.

4.0 ENERGY MODELS AND SOLUTION METHOD

One of the primary objectives of a spent fuel storage system is to remove decay heat from the fuel and maintain it within certain temperature limits. The heat is typically removed by a combination of the three primary modes of conduction, convection, and radiation heat transfer. To predict the temperature field within the storage system, the COBRA-SFS code must accurately model each mode.

In this section, the finite-volume energy equations and solution method are described in detail. The derivation of the conservation of energy equations for the fluid, solid structures and fuel rods is demonstrated in Section 4.1. The method for solving the equations is presented in Section 4.2. The constitutive models for heat transfer are presented in Section 4.3. The choice of thermal boundary conditions are described in Section 4.4.

4.1 CONSERVATION EQUATIONS

A typical spent fuel storage system may be divided into three regions: the cooling fluid, the solid structure and the spent fuel rods. For a typical spent fuel dry storage cask the cooling fluid would be the naturally circulating gas within the cask and the solid structure would be the assembly basket and cask body. To derive the conservation of energy equations for each of the regions, an energy balance is performed on the appropriate control volume. The derivation of the energy balance is presented below for each region.

4.1.1 Fluid Energy

The control volume used to derive the conservation of fluid energy equation is the standard subchannel control volume described in Section 3.1 and shown again in Figure 4.1. In a finite-volume formulation, the subchannel control volume is represented by a computational cell as shown in Figure 4.2. The computational variables are located on the cell as shown. The state variables of density (ρ) and enthalpy (h) are defined at the cell center and are indexed by the node number. The axial flow rate (m), pressure (P), and area (A) are

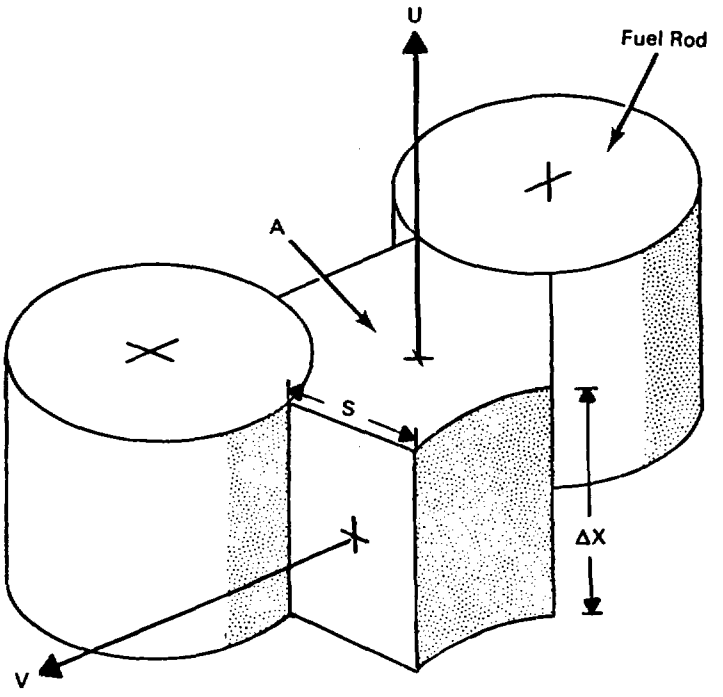

FIGURE 4.1. Subchannel Control Volume

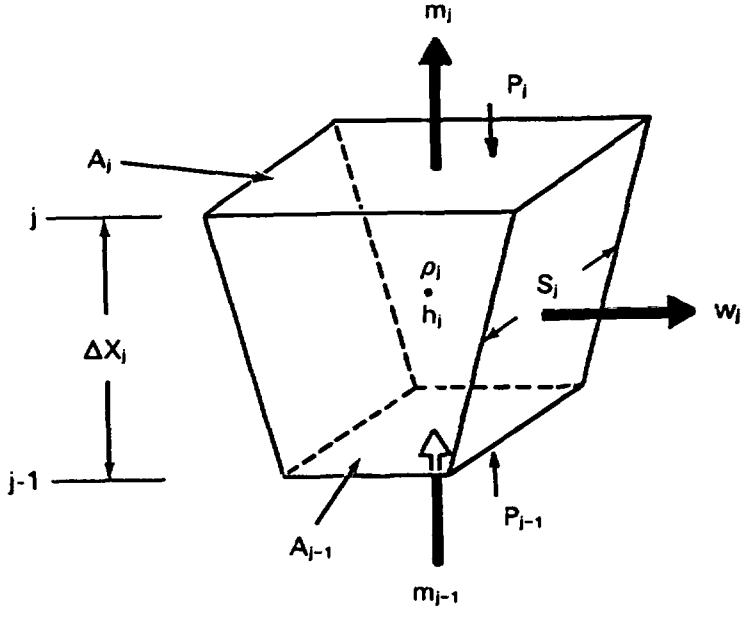

FIGURE 4.2. Subchannel Computational Cell

located at the axial cell boundaries and are indexed by the corresponding node and axial level. The crossflow per unit length, w, and gap width, S, are placed on the transverse cell boundaries midway between the axial levels and are indexed by the gap and axial level. In the difference equations, the positions of the variables are indicated by the axial index, j, j+1, j-1, etc.

The axial and transverse convection terms involve the transporting of enthalpy, located at the cell centers, by flows defined at the cell surfaces. It is assumed that the enthalpy being transported is equivalent to that of the donor cell, i.e., the cell from which the flow originates. For example, the finite-volume form of the axial convection term is

$$A\,(\rho Uh)_{x+\Delta x} - A\,(\rho Uh)_x = m_j h^* - m_{j-1}\,h^* \qquad (4.1)$$

where h^* is the donor cell enthalpy.

The fluid energy equation is derived by performing an energy balance on the control volume shown in Figure 4.2 and assuming that flow work is negligible. The balance includes terms describing both axial and lateral convective transport of fluid energy as well as an energy storage term. In addition, energy may enter the subchannel fluid from connecting fuel rods, Q_{FR}, solid surfaces, Q_{FW}, or by fluid conduction, Q_{FF}, and turbulent mixing from adjacent channels, Q_{FT}. The fluid energy balance is written as:

$$\bar{A}\,\Delta x\,\frac{\rho h - (\rho h)^n}{\Delta t} + m_j h^* - m_{j-1} h^* + \sum_{k\epsilon\Psi_i} e_{ik}\,w_j h^* = Q_{FR} + Q_{FW} + Q_{FF} + Q_{FT} \qquad (4.2)$$

The crossflow, w, is directed by its gap such that positive crossflow is defined to be from channel ii to channel jj, where ii is the smaller index. To account for this, the switch function, e_{ik}, is used as multiplier on the crossflow where

$$e_{ik} = \begin{cases} 1 \text{ if the channel index, i, is equal to ii} \\ -1 \text{ if the channel index, i, is equal to jj} \end{cases}$$

Therefore $e_{ik} = 1$ indicates that positive crossflow is out of channel i and $e_{ik} = -1$ indicates that positive crossflow is into channel i. The total heat entering from the fuel rods is defined as

$$Q_{FR} = \sum_{n \epsilon \lambda_i} P_R \, \Phi_i \, \Delta x \, q_c'' \tag{4.3}$$

where the summation is over the set, λ_i, of all rods, n, facing the control volume, i. P_R is the perimeter of the rod n, Φ is the fraction of the rod perimeter connected to the control volume, and q_c'' is the convection heat flux. The total heat entering from the connecting solid surfaces can be defined in the same manner as

$$Q_{FW} = \sum_{m \epsilon \tau_i} P_w \, \Delta x \, q_c'' \tag{4.4}$$

where the summation is over the set, τ_i, of all solid surfaces, m, adjacent to control volume, i; P_w is the connecting perimeter of surface m; and q_c'' is the convective heat flux.

For terms in the fluid energy equation that involve convection heat transfer through the solid surfaces, the surface-averaged convection heat flux, q_c'', is modeled using a heat transfer coefficient, H_{surf}, such that

$$q_c'' = H_{surf} \, (T_s - T) \tag{4.5}$$

where T_s is the rod or slab surface temperature. Therefore,

$$\Delta x \sum_{n \epsilon \lambda_i} P_R \, \Phi_i \, q_c'' = \Delta x \sum_{n \epsilon \lambda_i} P_R \, \Phi_i \, H_{surf} \, (T_{c_n} - T) \tag{4.6}$$

and

$$\Delta x \sum_{m \epsilon \tau_i} P_w \, q_c'' = \Delta x \sum_{m \epsilon \tau_i} P_w \, H_w \, (T_{w_m} - T) \tag{4.7}$$

where T_c and T_w are the clad and slab temperatures, respectively. When a rod model is not used, q''_c is simply

$$q''_c = \frac{A_f}{P_R} q''' \tag{4.8}$$

where A_f is the cross sectional area of the fuel and q''' is the volumetric heat generation rate of the fuel.

The total heat entering by fluid conduction from adjacent subchannels is defined as

$$Q_{FF} = \sum_{k \epsilon \Psi_i} S\Delta x \, q''_k \tag{4.9}$$

where the summation is over all gaps, k, connecting the control volume, i, S is the gap width, and q''_k is the fluid conduction heat flux.

The heat flux from fluid conduction, q''_k, between adjacent subchannels is based on the gap width, S, and conduction length, ℓ_c, defined as

$$\ell_c = \ell \, Z_k \tag{4.10}$$

where ℓ is the transverse control volume length and Z_k is an empirically determined conduction shape factor. Equation (4.9) then becomes

$$Q_{FF} = \Delta x \sum_{k \epsilon \Psi_i} S_k \, q''_k = \Delta x \sum_{k \epsilon \Psi_i} S_k e_{ik} k_k \frac{(T_{ii} - T_{jj})}{\ell \, Z_k} \tag{4.11}$$

where k_k is the average fluid thermal conductivity based on channel fluid temperature from the previous iteration.

Turbulence in the flow field mixes the fluid in adjacent subchannels through the gap. This mixing results in the transfer of fluid energy from one subchannel to another. To determine the amount of transfer that occurs,

a turbulent exchange crossflow, w_T, is calculated as a function of flow and other parameters. A selection of different expressions used to calculate the turbulent exchange crossflow is described in Section 3.4.3. The turbulent energy exchange between subchannels is expressed as

$$Q_{FT} = \sum_{k\epsilon\Psi_i} w_T \, (h_{ii} - h_{jj}) \tag{4.12}$$

When all the terms are combined, the following conservation of fluid energy equation is obtained:

$$\bar{A}\,\Delta x \,\frac{\rho h - (\rho h)^n}{\Delta t} + m_j h^* - m_{j-1} h^* + \sum_{k\epsilon\Psi_i} e_{ik}\, w_j h^*$$

$$\left[\text{energy storage}\right] + \left[\begin{matrix}\text{energy transported}\\ \text{axially}\end{matrix}\right] + \left[\begin{matrix}\text{energy transported}\\ \text{laterally}\end{matrix}\right]$$

$$= \Delta x \sum_{n\epsilon\lambda_i} P_R \, \Phi_i \, H_{surf} \, (T_{c_n} - T) + \Delta x \sum_{m\epsilon\tau_i} P_w \, H_w \, (T_{w_m} - T)$$

$$= \text{[rod heat input]} + \text{[slab heat input]}$$

$$+ \Delta x \sum_{k\epsilon\Psi_i} \epsilon_{ik} \, S_k \, k_k \, \frac{(T_{ii} - T_{jj})}{\ell \, Z_k} + \sum_{k\epsilon\Psi_i} e_{ik} \, w_T \, (h_{ii} - h_{jj})_k \tag{4.13}$$

$$+ \text{[fluid conduction laterally]} + \text{[turbulent energy exchange]}$$

In this derivation, it is assumed that there is no fluid conduction in the axial direction. All other forms of energy that are not explicitly represented in Equation (4.13) (such as potential and kinetic energy) are assumed to be negligible.

4.1.2 Solid Structure Energy

Conduction through solid structures plays a significant role in many heat transfer problems. For a dry storage cask, heat is removed by conduction

through the assembly basket and cask body. Therefore, an equation for the conservation of energy in solid structures is required to model the solid-to-solid and solid-to-fluid heat transfer.

The control volume used in the solid conservation of energy equation, which hereafter will be referred to as a "slab", is shown in Figure 4.3. The axial length of the control volume is denoted by Δx, which corresponds to that used for the fluid subchannels, and the cross-sectional area is denoted by A. The control volume may have any number of surfaces connected to adjacent slabs or fluid subchannels in the lateral direction. In addition to conduction and convection heat transfer, the control volume may exchange energy by thermal radiation with the surfaces of fuel rods and other slabs. The slab control volume is similar to the subchannel control volume in that it allows a great deal of flexibility in modeling heat transfer problems, since it is not constrained by a fixed coordinate system.

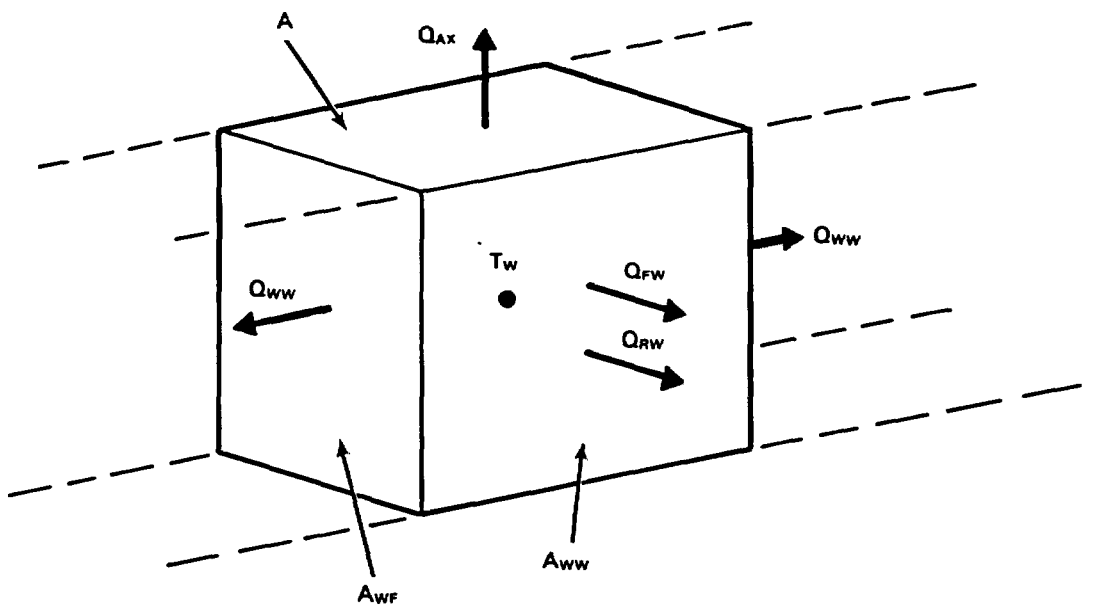

FIGURE 4.3. Solid Control Volume

The slab conservation of energy equation consists of an energy storage term and a series of terms describing energy transferred from subchannels, other slabs and rods. The total energy from adjacent subchannels, Q_{FW}, is transferred soley by convection. The total energy from other slabs, Q_{WW}, is transferred by both conduction and radiation. The total energy from fuel rods, Q_{RW}, is transferred solely by radiation. When these terms are added, the conservation of solid energy equation may be written as:

$$A\,\Delta x\,\rho_w c_w \frac{T_w - T_w^n}{\Delta t} = - Q_{FW} - Q_{WW} - Q_{RW} \tag{4.14}$$

where T_w is the slab temperature.

Using the definitions provided in Section 4.1.1, the total energy from adjacent subchannels is described by

$$Q_{FW} = \Delta x \sum_{\ell \epsilon \xi_i} P_w H_w (T_w - T_\ell) \tag{4.15}$$

where the summation is over the set, ξ_i, of all subchannels, ℓ, connected to slab control volume i; P_w is the wetted perimeter; and H_w is the heat transfer coefficient.

The total heat entering the reference control volume, i, from adjacent slabs by conduction and radiation is defined as

$$Q_{WW} = \sum_{m \epsilon \alpha_i} A_{WW}\, q''_k + \sum_{m \epsilon \sigma_i} A_{WF}\, q''_{RW} + Q_{AX} \tag{4.16}$$

$$\left[\begin{array}{l}\text{transverse} \\ \text{conduction}\end{array}\right] + [\text{radiation}] + [\text{axial conduction}]$$

where the summation in the first term is over the set, α_i, of all slab control volumes m, with a conduction connection to control volume i; A_{WW} is the connecting area; and q''_k is the conduction heat flux.

Radiation is assumed to be confined to two dimensions so that only the slab and fuel rod surfaces on the current axial level are considered. The summation in the second term is over the set, σ_i, of all slab control volumes, m, connected to the control volume i, by radiation. A_{WF} is the radiations surface area of slab i and q''_{RW} is the net radiation heat flux from the slab.

In addition to heat transfer in the lateral direction, the heat transferred in the axial direction by solid conduction is defined as

$$Q_{AX} = (A\ q''_x)_j + (A\ q''_x)_{j-1} \tag{4.17}$$

where surface A is the slab cross-sectional area and q''_x is the axial conduction heat flux at the top and bottom surfaces.

The solid conduction between adjacent slabs, q''_k, is modeled using a composite thermal conductance, U, which accounts for the heat transfer area, the thermal conductivity of the slab materials, and any gap resistance or thermal radiation at the slab interface. Therefore,

$$\sum_{m\epsilon\alpha_i} A_{WW}\ q''_k = \sum_{m\epsilon\alpha_i} U\ (T_w - T_{w_m}) \tag{4.18}$$

and

$$(A\ q''_x)_j + (A\ q''_x)_{j-1} = U_j\ (T_w - T_{w_{j+1}}) + U_{j-1}\ (T_w - T_{w_{j-1}}) \tag{4.19}$$

where U_j and U_{j-1} are the composite thermal conductances through the top and bottom of the slab, respectively. The calculation of composite thermal conductances, U, is described in more detail in Section 4.3.3. The total heat entering from fuel rods by radiation is defined as

$$Q_{RW} = \sum_{n\epsilon\kappa_i} A_{WF}\ q''_{RR} \tag{4.20}$$

where the summation is over all fuel rods, n, connected to the control volume, i, by radiation. A_{WF} is the radiations surface area of slab i and q''_{RR} is the heat flux from each rod.

The radiation heat transfer from one surface to another is calculated using the expression

$$q''_{RR} = \sigma F_{1-2} (T_1^4 - T_2^4) \tag{4.21}$$

where F_{1-2} is the gray body radiation exchange factor based on geometry and surface emissivities and σ is the Stefan-Boltzmann constant. Using this expression, the radiation heat transfer from slabs and rods is

$$\sum_{m \epsilon \sigma_i} A_{WF} q''_{RW} = \sum_{m \epsilon \sigma_i} A_{WF} \sigma F_{im} (T_w^4 - T_{w_m}^4) \tag{4.22}$$

where T_{wm} is the temperature of slab m, and

$$\sum_{n \epsilon \kappa_i} A_{WF} q''_{RR} = \sum_{n \epsilon \kappa_i} A_{WF} \sigma F_{in} (T_w^4 - T_{c_n}^4) \tag{4.23}$$

where T_{c_n} is the cladding temperature of rod n. The calculation of radiation exchange factors, F, is described in detail in Section 4.4.4.

When all the terms are combined, the solid structure energy conservation equation is

$$A\,\Delta x\,\rho_w c_w \frac{T_w - T_w^n}{\Delta t} = -U_j\,(T_w - T_{w_{j+1}}) - U_{j-1}\,(T_w - T_{w_{j-1}})$$

[energy storage] = [axial heat conduction]

$$- \sum_{m\epsilon\alpha_i} U\,(T_w - T_{w_m}) - \sum_{m\epsilon\sigma_i} A_{WF}\,\sigma\,F_{im}\,(T_w^4 - T_{w_m}^4)$$

$$- \left[\begin{matrix}\text{lateral heat}\\ \text{conduction}\end{matrix}\right] - \left[\begin{matrix}\text{radiation heat transfer}\\ \text{from slabs}\end{matrix}\right]$$

$$- \sum_{n\epsilon\kappa_i} A_{WF}\,\sigma\,F_{in}\,(T_w^4 - T_{c_n}^4) - \Delta x \sum_{\ell\epsilon\xi_i} P_w\,H_w\,(T_w - T_\ell) + \Delta x\,A\,q''' \qquad (4.24)$$

$$\left[\begin{matrix}\text{radiation heat transfer}\\ \text{from rods}\end{matrix}\right] - \left[\begin{matrix}\text{convection heat}\\ \text{transfer}\end{matrix}\right] + \text{[heat generation]}$$

4.1.3 Rod Energy

The spent nuclear fuel rods in storage generate decay heat that must be efficiently removed to maintain acceptable fuel rod temperatures. The heat transfer from the rods is modeled in three different ways.

The first, which is the simplest method of distributing the heat generated in a fuel rod, is to assume a constant heat flux around the periphery of the rod while neglecting transient effects and thermal radiation. The total heat is distributed to the surrounding channels according to the fraction of the rod perimeter, Φ_ℓ, adjacent to each channel so that the convection term in the fluid energy Equation (4.3) for channel ℓ becomes

$$Q_{FR} = \sum_{\ell\epsilon\gamma_i} P_R\,\Phi_\ell\,\Delta x\,q_c'' \qquad (4.25)$$

where q''_c is simply

$$q''_c = \frac{A_f}{P_r} q''' \tag{4.8}$$

and A_f is the cross sectional area of the fuel and q''' is the fuel volumetric heat generation rate.

The second method is used for most steady-state spent fuel problems where the effect of thermal radiation is important. This rod model was developed to provide clad surface temperatures for determining convection and radiation heat transfer.

The total heat removed by convection is defined as before in Equation (4.25) but q''_c varies as a function of fluid temperature [see Equation (4.5)]. The radiation term includes contributions from slabs and other rods within the same assembly. By assuming that only slabs and rod surfaces on the same axial level exchange radiant energy, the net radiant heat transfer from other fuel rods by radiation is defined as

$$Q_{RR} = \sum_{n \epsilon \varsigma_i} P_R \Delta x \, (q''_r)_n \tag{4.26}$$

where the summation is over the set, ς_i, of all fuel rods within an assembly radiating to rod i, P_R is the rod perimeter, and $(q''_r)_n$ is the net radiant heat flux from each rod. The total heat flux entering from slabs by radiation is defined as

$$Q_{RW} = \sum_{m \epsilon \beta_i} P_R \Delta x \, (q''_r)_m \tag{4.27}$$

where the summation is over the set, β_i, of all slabs, m, connected to rod i by radiation. The term $(q''_r)_m$ is the net radiant heat flux from each slab.

The rod energy conservation equation for the second model takes the form

$$0 = -\Delta x \sum_{\ell \epsilon \gamma_i} P_R \Phi_\ell H_{surf} (T_c - T_\ell) - \Delta x \sum_{n \epsilon \varsigma_i} P_R \sigma F_{in} (T_c^4 - T_{c_n}^4)$$

$$- \left[\begin{array}{l}\text{convection heat transfer} \\ \text{with fluid}\end{array}\right] \qquad - \left[\begin{array}{l}\text{radiation heat transfer} \\ \text{between rods}\end{array}\right]$$

$$- \Delta x \sum_{m \epsilon \beta_i} P_R \sigma F_{im} (T_c^4 - T_{w_m}^4) + A_f \Delta x \, q''' \qquad (4.28)$$

$$- \left[\begin{array}{l}\text{radiation heat transfer} \\ \text{from slabs}\end{array}\right] + [\text{heat generation}]$$

where A_f is the cross-sectional area of the fuel and q''' is the fuel volumetric heat generation rate. In this derivation, it is assumed that there is no axial heat transfer, and that the temperature is uniform around the circumference of the cladding.

The third model is used for transient calculations. In this model, separate energy equations are written for the clad and the fuel energy. The fuel rod is divided into one clad node and several fuel nodes as shown in either Figure 4.4 when a central void is present or Figure 4.5 when there is no central void. The innermost and outermost fuel nodes are one-half the thickness of the other nodes. The cladding energy equation is obtained by performing a lumped energy balance on the cladding material at each axial level. The clad energy conservation equation is written as

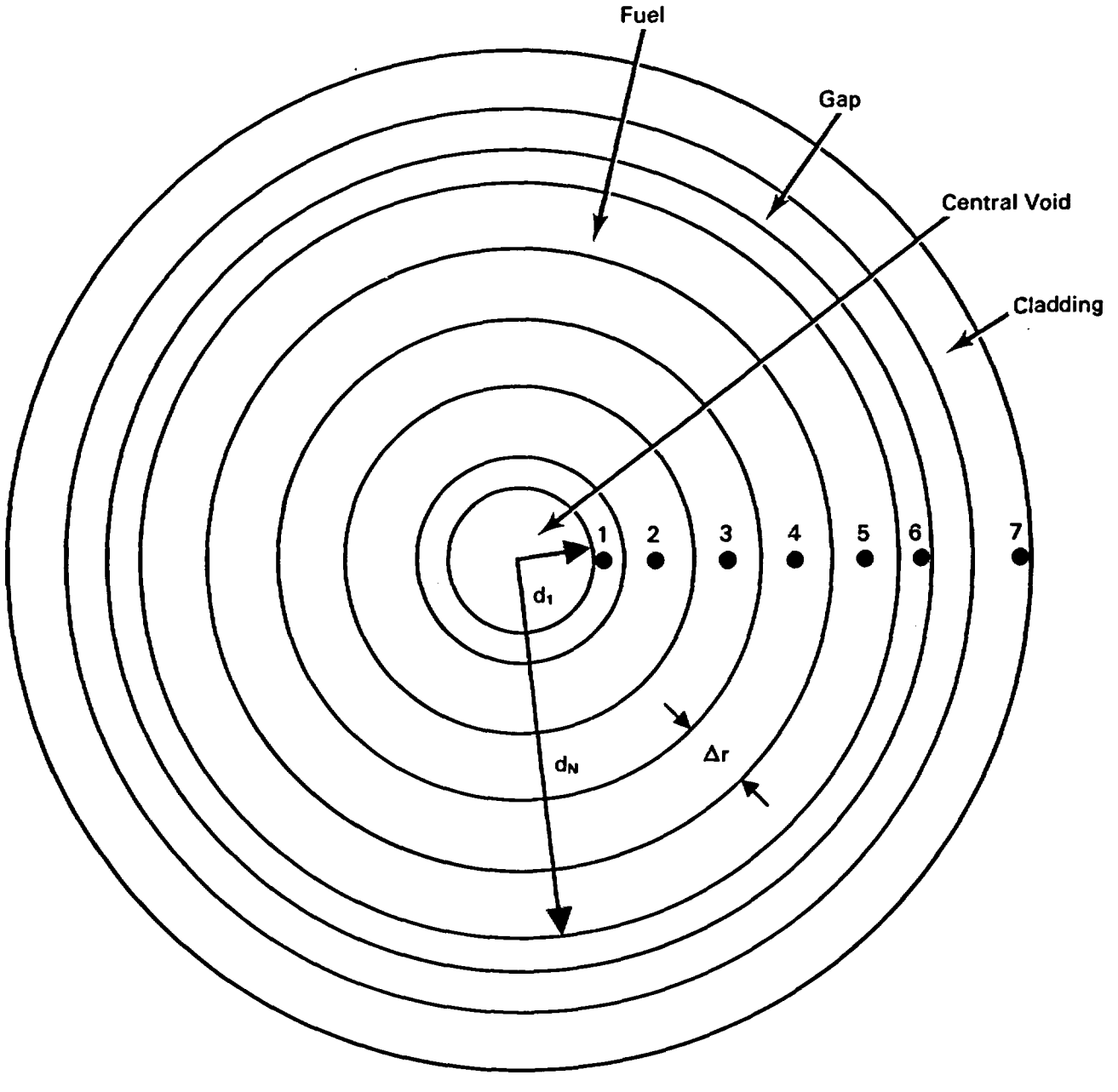

FIGURE 4.4. COBRA-SFS Finite-Volume Fuel Rod Model with Central Void

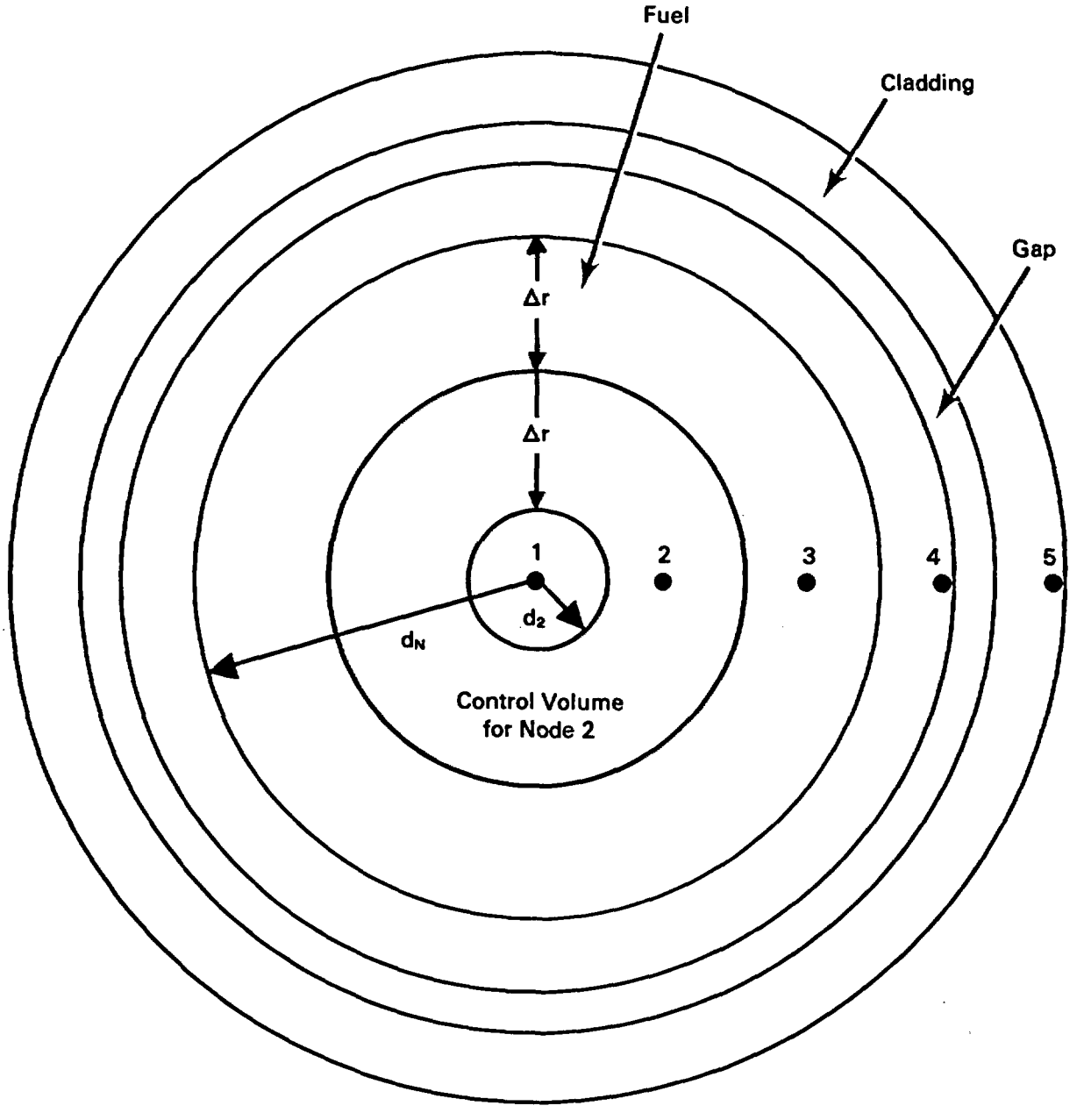

FIGURE 4.5. COBRA-SFS Finite-Volume Fuel Rod Model Without Central Void

$$A_c \Delta_x \rho_c C_c \frac{T_c - T_c^n}{\Delta t} = -\sum_{\ell \epsilon \gamma_i} P_R \Phi_\ell \Delta x \, q_c'' - \sum_{n \epsilon \zeta_i} P_R \Delta x \, q_r''$$

$$[\text{energy storage}] = \left[\begin{matrix}\text{convection} \\ \text{heat transfer}\end{matrix}\right] - \left[\begin{matrix}\text{rod radiation} \\ \text{heat transfer}\end{matrix}\right]$$

$$- \sum_{m \epsilon \beta_i} P_R \Delta x \, q_r'' - P_f \Delta x \, q_g'' \qquad (4.29)$$

$$- \left[\begin{matrix}\text{slab radiation} \\ \text{heat transfer}\end{matrix}\right] - [\text{heat transfer from fuel}]$$

where P_f is the perimeter of the fuel and q_g'' is the surface averaged heat flux across the gap. The only term not defined in the composite rod model is the heat transfer from the fuel to the clad. The fuel surface-averaged gap heat flux, q_g'', is modeled using a gap heat transfer coefficient, Hg, such that

$$q_g'' = Hg \, (T_c - T_{fs}) \qquad (4.30)$$

where d_{fuel} is the fuel diameter and T_{fs} is the fuel surface temperature.

Solid conduction within the fuel is modeled in both the radial and circumferential directions with the variable N_θ indicating the number of circumferential sections the fuel rod is divided into. The temperatures are identified as $T_{k,m}$ where k is the radial location and m is the circumferential location. The finite-volume equations for each of the N fuel nodes and the cladding node, N+1, are as follows:

Node 1 (inner node):

$$\pi\left(\frac{d_2^2 - d_{void}^2}{4N_\theta}\right)\rho_f c_f \frac{T_{1,m} - T_{1,m}^n}{\Delta t} + \frac{\pi d_2}{\Delta r N_\theta} k_f (T_{1,m} - T_{2,m})$$

$$+ \frac{2\Delta r N_\theta}{\pi(d_1+d_2)} k_f (2T_{1,m} - T_{1,m-1} - T_{1,m+1}) \qquad (4.31)$$

$$= q_f''' \pi\left(\frac{d_2^2 - d^2{}_1}{4N_\theta}\right) + \frac{\pi}{N_\theta} d_1 q''_{void}$$

Nodes 2 through N-1:

$$\pi\left(\frac{d_{k+1}^2 - d_k^2}{4N_\theta}\right)\rho_f c_f \frac{T_{k,m} - T_{k,m}^n}{\Delta t} + \frac{\pi d_k}{\Delta r N_\theta} k_f (T_{k,m} - T_{k-1,m}) + \frac{\pi d_{k+1}}{\Delta r N_\theta} (T_{k,m} - T_{k+1,m})$$

$$+ \frac{2\Delta r N_\theta}{\pi(d_k + d_{k+1})} k_f (2T_{k,m} - T_{k,m-1} - T_{k,m+1}) = q'''_f \pi\left(\frac{d_{k+1}^2 - d^2{}_k}{4N_\theta}\right) \qquad (4.32)$$

Node N:

$$\pi\left(\frac{d_{fuel}^2 - d_N^2}{4N_\theta}\right)\rho_f c_f \frac{T_{N,m} - T_{N,m}^n}{\Delta t} + \frac{\pi d_N}{\Delta r N_\theta} k_f (T_{N,m} - T_{N-1,m}) + \frac{\pi d_{fuel} H_g}{N_\theta} (T_{N,m} - T_{c,m})$$

$$+ \frac{2\Delta r N_\theta}{\pi(d_{fuel} + d_N)} (2T_{n,m} - T_{n,m-1} - T_{n,m+1}) = q'''_f \pi\left(\frac{d_{fuel}^2 - d_N^2}{4N_\theta}\right) \qquad (4.33)$$

Clad Node:

$$\pi\left[\frac{d_{clad}^2 - (d_{clad} - 2t_{clad})^2}{4N_\theta}\right]\rho_c c_c \frac{T_{c,m} - T_{c,m}^n}{\Delta t} + \pi \frac{d_{fuel} H_g}{N_\theta}(T_{c,m} - T_{N,m})$$

$$+ \frac{\pi d_{clad} H_{surf}}{N_\theta}(T_{c,m} - T_{fluid,m}) + \frac{\Delta r N_\theta k_c}{\pi(d_{clad} - t_{clad})}(2T_{c,m} - T_{c,m-1} - T_{c,m+1})$$

$$+ \sum_{n\epsilon\zeta_i} P_R \sigma F_{in}(T_{c,m}^4 - T_{c,n}^4) + \sum_{m\epsilon\beta_i} P_R \sigma F_{im}(T_{c,m}^4 - T_{w,m}^4) = 0 \qquad (4.34)$$

In this derivation it is assumed that there is no axial heat transfer, the heat is generated uniformly throughout the fuel at a given axial location and the fuel properties do not vary with the radial variation in temperature.

4.2 ENERGY SOLUTION METHOD

The finite-volume energy equations presented in Section 4.1 are written for each channel, rod, and structural node on an axial level. The energy solution is divided into three parts: 1) the coefficient matrices representing the individual rod equations are decomposed by lower-upper (LU) triangular factorization to determine T_{clad} as a function of T_{fluid}, 2) the fluid and slab equations are solved simultaneously using successive overrelaxation to obtain a fluid enthalpy and slab temperature distribution, and 3) the rod temperature distribution is determined by back substitution of the new fluid temperatures. The rod coefficient matrix factorization is described in more detail in Section 4.2.1 and the fluid and slab energy solution is described in Section 4.2.2.

4.2.1 Rod Energy Equation Decomposition

To expedite the energy solution, the rod surface temperature is described as a function of fluid temperature in the form

$$T_{clad} = K_1 + K_2 + K_3 H_{surf} T_{fluid} \qquad (4.35)$$

where the constants K_1, K_2, and K_3 are generated by performing an LU decomposition on the fuel rod finite-volume equations. If radiation heat transfer is not considered, the constants are generated only once. If radiation is considered, the clad temperature of a particular rod is dependent on the temperatures of other rods and the rod equations are solved iteratively using the fluid and slab temperature distribution from the previous fluid temperature iteration. When the constants K_1, K_2, and K_3 have been determined, the expression for clad temperature [Equation (4.35)] is substituted into the fluid energy equation [Equation (4.13)] prior to solving the fluid and slab energy equations.

In order to perform the decomposition, the fuel rod finite-volume equations [Equations (4.31) through (4.34)] are cast into a tridiagonal matrix of the form shown in Equation (4.36). Here a rod model with one clad node and four fuel nodes is used as an example.

$$\begin{bmatrix} A_{12} & A_{13} & 0 & 0 & 0 \\ A_{21} & A_{22} & A_{23} & 0 & 0 \\ 0 & A_{31} & A_{32} & A_{33} & 0 \\ 0 & 0 & A_{41} & A_{42} & A_{43} \\ 0 & 0 & 0 & A_{51} & A_{52} \end{bmatrix} \quad \begin{Bmatrix} T_1 \\ T_2 \\ T_3 \\ T_4 \\ T_{clad} \end{Bmatrix} = \begin{Bmatrix} Y_1 \\ Y_2 \\ Y_3 \\ Y_4 \\ Y_5 + f(T_f) \end{Bmatrix} \qquad (4.36)$$

The elements are ordered in a manner that allows storage of the coefficients in a 3 x 5 array. Thus the subscripts are the index values of the storage array in COBRA-SFS rather than the matrix index.

The terms in the coefficient matrix A are defined in Table 4.1 and the terms in the source vector Y are defined in Table 4.2. If the coolant temperature distribution T_f was known, Equation (4.36) could be solved for the rod temperature distribution. However, since T_f is unknown, matrix A is factored into a lower |C| and upper |B| triangular matrix as shown in Equation (4.37). Again the subscripts represent storage locations rather than matrix indices.

$$\bar{A} = \begin{bmatrix} 1 & 0 & 0 & 0 & 0 \\ C_{21} & 1 & 0 & 0 & 0 \\ 0 & C_{31} & 1 & 0 & 0 \\ 0 & 0 & C_{41} & 1 & 0 \\ 0 & 0 & 0 & C_{51} & 1 \end{bmatrix} \begin{bmatrix} B_{11} & B_{12} & 0 & 0 & 0 \\ 0 & B_{21} & B_{22} & 0 & 0 \\ 0 & 0 & B_{31} & B_{32} & 0 \\ 0 & 0 & 0 & B_{41} & B_{42} \\ 0 & 0 & 0 & 0 & B_{51} \end{bmatrix} \tag{4.37}$$

Performing the indicated matrix multiplication gives:

$$\overline{CB} = \begin{bmatrix} B_{11} & B_{12} & 0 & 0 & 0 \\ C_{21}B_{11} & C_{21}B_{12}+B_{21} & B_{22} & 0 & 0 \\ 0 & C_{31}B_{21} & C_{31}B_{22}+B_{31} & B_{32} & 0 \\ 0 & 0 & C_{41}B_{31} & C_{41}B_{32}+B_{41} & B_{42} \\ 0 & 0 & 0 & C_{51}B_{41} & C_{51}B_{42}+B_{51} \end{bmatrix} \tag{4.38}$$

By inspection, the terms of the stored A matrix can be defined in terms of the B and C matrices as:

$$\begin{array}{lll} & A_{12} = B_{11} & A_{13} = B_{12} \\ A_{21} = C_{21}B_{21} & A_{22} = C_{21}B_{12}+B_{21} & A_{23} = B_{22} \\ A_{31} = C_{31}B_{21} & A_{32} = C_{31}B_{22}+B_{31} & A_{33} = B_{32} \\ A_{41} = C_{41}B_{31} & A_{42} = C_{41}B_{32}+B_{41} & A_{43} = B_{42} \\ A_{51} = C_{51}B_{41} & A_{52} = C_{51}B_{42}+B_{51} & A_{53} = 0 \end{array} \tag{4.39}$$

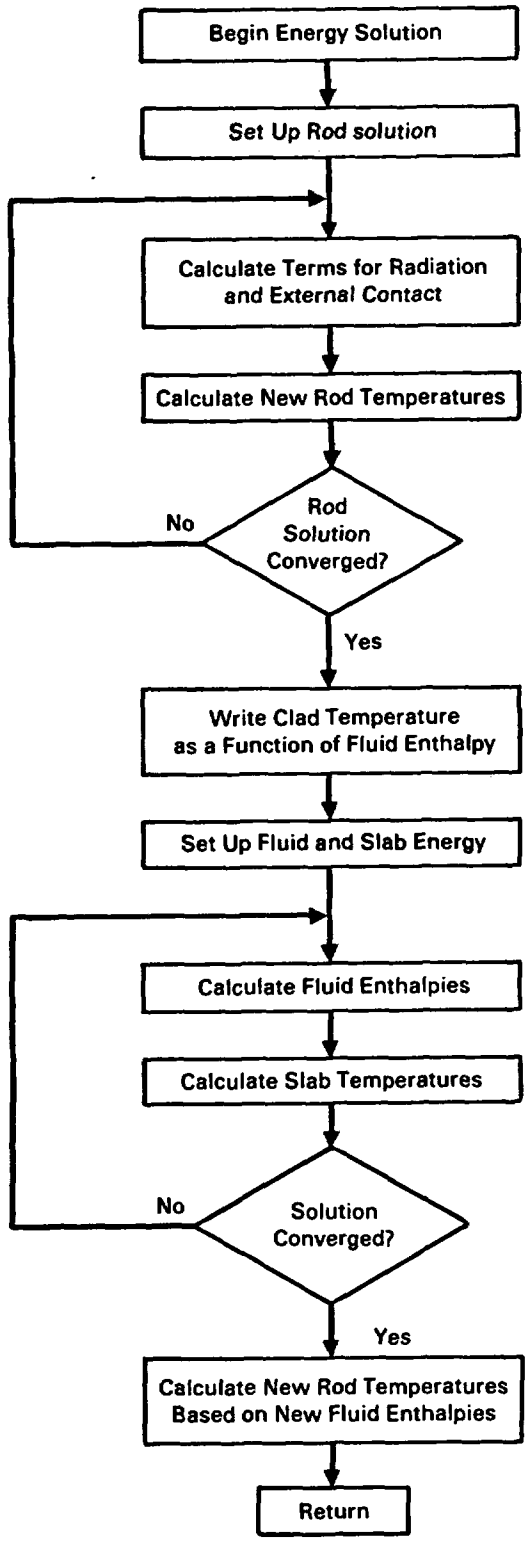

FIGURE 4.6. Flow Chart of Energy Solution Scheme

TABLE 4.1. Definitions of Coefficients in the A Matrix

Element	Definition
A_{12}	$\frac{(\rho c)_f}{\Delta t}\left(\frac{d_2^2 - d_{void}^2}{4N_\theta}\right) + \frac{d_2}{\Delta r N_\theta} k_f + \frac{4\Delta r N_\theta k_f}{\pi^2(d_1+d_2)}$
A_{13}	$-\frac{d_2}{\Delta r N_\theta} k_f$
A_{21} and A_{31}	$-\frac{d_i}{\Delta r N_\theta} k_f$
A_{22} and A_{32}	$\frac{(\rho c)_f}{\Delta t}\left(\frac{d_{i+1}^2 - d_i^2}{4N_\theta}\right) + \frac{k_c}{\Delta r N_\theta}(d_i + d_{i+1}) + \frac{4\Delta r N_\theta k_f}{\pi^2(d_i + d_{i+1})}$
A_{23} and A_{33}	$-\frac{d_{i+1}}{\Delta r N_\theta} k_f$
A_{41}	$-\frac{d_N}{\Delta r N_\theta} k_f$
A_{42}	$\frac{(\rho c)_f}{\Delta t}\left(\frac{d_{fuel}^2 - d_N^2}{4N_\theta}\right) + \frac{d_N}{\Delta r N_\theta} k_f + \frac{d_{fuel} H_g}{N_\theta} + \frac{4\Delta r N_\theta k_f}{\pi^2(d_{fuel} + d_n)}$
A_{43} and A_{51}	$-\frac{d_{fuel} H_g}{N_\theta}$
A_{52}	$\frac{(\rho c)_{clad}}{\Delta t}\left[\frac{d_{clad}^2 - (d_{clad} - 2t_{clad})}{N_\theta}\right]^2 + \frac{d_{fuel} H_g}{N_\theta} + \frac{d_{clad} H_{surf}}{N_\theta} + \frac{2\Delta r N_\theta k_c}{\pi^2(d_{clad} - t_{clad})}$

TABLE 4.2. Definitions of Terms in the Y Matrix

Element	Definition
Y_1	$\left[\frac{(\rho c)_f T_1^n}{\Delta t} + q_f'''\right]\left(\frac{d_1^2 - d_{void}^2}{4N_\theta}\right) + \frac{d_{void}}{N_\theta} q''_{void} + \frac{2\Delta_r N_\theta k_f}{\pi^2(d_1+d_2)} (T_{1,m-1} + T_{1,m+1})$
Y_2, Y_3 and Y_4	$\left[\frac{(\rho c)_f T_1^n}{\Delta t} + q_f'''\right]\left(\frac{d_i^2 - d_{i-1}^2}{4N_\theta}\right) + \frac{2\Delta r N_\theta k_f}{\pi^2(d_i + d_{i+1})} (T_{n,m-1} + T_{n,m+1})$
Y_5	$\left[\frac{(\rho c)_f T_c^n}{\Delta t} + q'''_{clad}\right]\left[\frac{d_{clad}^2 - (d_{clad} - 2t_{clad})^2}{4N_\theta}\right] + \frac{\Delta r N_\theta k_c}{\pi^2(d_{clad} - t_{clad})} (T_{c,m+1} + T_{c,m-1})$
$f(T_f)$	$(d_5 H_{surf} T_{fluid})$

Using elementary matrix algebra an algebraic expression relating Tclad and Tfluid can be determined:

$$\begin{aligned} &\text{let} && \bar{A}T = Y \\ &\text{and} && Y = \bar{C}Z \\ &\text{then} && \bar{C}\bar{B}T = Y \\ & && \bar{C}\bar{B}T = \bar{C}Z \\ &\text{thus} && \bar{B}T = Z \end{aligned} \qquad (4.40)$$

Since $\bar{B}$ is upper triangular, only Z must be found to solve for T. The elements of $\bar{C}$ and $\bar{B}$ are given below:

$$
\begin{aligned}
& & C_{21} &= A_{21}/B_{11} \\
B_{11} &= A_{12} & B_{21} &= A_{21}/C_{21} \\
B_{12} &= A_{13} & B_{22} &= A_{23} \\
C_{31} &= A_{31}/B_{21} & C_{41} &= A_{41}/B_{31} \\
B_{31} &= A_{32} - C_{31}B_{22} & B_{41} &= A_{42} - C_{41}B_{32} \\
B_{32} &= A_{33} & C_{42} &= A_{43} \\
C_{41} &= A_{51}/B_{41}
\end{aligned}
\tag{4.41}
$$

Since $Y = \bar{C}Z$, Z can be evaluated in terms of C and Y as:

$$
\begin{aligned}
Z_1 &= Y_1 \\
Z_2 &= Y_2 - Z_1C_{21} \\
Z_3 &= Y_3 - Z_2C_{31} \\
Z_4 &= Y_4 - Z_3C_{41} \\
Z_5 &= Y_5 - Z_4C_{51} + f(T_f)
\end{aligned}
\tag{4.42}
$$

Since BT = Z, the expression for the clad temperature is determined as:

$$B_{51}\ T_5 = Z_5 \tag{4.43}$$

$$T_5 = Z_5/B_{51} \tag{4.44}$$

$$T_5 = \frac{Y_5}{B_{51}} + \frac{Z_4C_{51}}{B_{51}} + \frac{d_5H_{surf}}{B_{51}}\ T_{fluid} \tag{4.45}$$

or in more general terms of N fuel nodes this is

$$T_{N+1} = \frac{Y_{N+1}}{B_{N+1}} + \frac{Z_N\ C_{N+1}}{B_{N+1}} + \frac{d_{rod}\ H_{surf}}{B_{N+1}}\ T_{fluid} \tag{4.46}$$

This is equivalent to the clad temperature expression

$$T_{clad} = K_1 + K_2 + K_3 H_{surf} T_{fluid} \quad (4.35)$$

This decomposition allows the clad and fuel temperatures to be expressed as functions of fluid temperature. If there is no thermal radiation heat transfer, circumferential conduction heat transfer or rod-to-rod contact in the problem, the rod solution is complete. However, if any of these effects are included, a change in temperature results in a change in the source matrix, Y, which requires iteration on the rod temperatures. When the constants K_1, K_2, and K_3 have been determined, the expression for clad temperature [Equation (4.35)] is substituted into the fluid energy equation [Equation (4.13)] prior to solving the fluid and slab energy equations.

4.2.2 Fluid and Slab Energy Solution

The finite-volume formulations for the fluid energy equation [Equation (4.13)] and the solid structure energy equation [Equation (4.24)] are written for every fluid and slab node at a particular axial level. The two sets are generally tightly coupled so that simultaneous solution of both sets is required. The construction of the matrix equation for each set is described below. A description of the solution for both sets follows.

The fluid energy equation [Equation (4.13)] is written in terms of fluid enthalpy. However, certain terms require the fluid temperature to calculate heat transfer due to fluid conduction and convection. The fluid temperatures are related to enthalpies by the following approximation.

$$T = T_o + \frac{h - h_o}{c} \quad (4.47)$$

where the reference temperature and enthalpy are chosen arbitrarily as the previous iteration values for T and h, and c is the fluid specific heat. The clad temperature, T_c, is represented by the expression developed in Section 4.2.1.

$$T_{clad} = K_1 + K_2 + K_3 H_{surf} T_{fluid} \quad (4.35)$$

When these two expressions are substituted into the fluid energy equation [Equation (4.13)], an equation is obtained that is linear in enthalpy. These equations, one for each subchannel at level j, are combined to form the matrix equation

$$[L]\ \{h\}_j = \{S_h\} \tag{4.48}$$

where [L] is an NxN coefficient matrix (N being the number of channels), $\{S_h\}$ is the source vector, and $\{h\}_j$ the fluid enthalpies at level j. For large problems the matrix [L] is sparse, therefore only the nonzero elements are stored.

The only temperature term in the fluid energy equation that is not expressed in terms of enthalpy is the slab temperature, T_w. These temperatures are obtained during the iteration from the slab energy equation and are represented in the source vector, $\{S_h\}$. After each slab energy iteration, the terms containing slab temperatures are updated to reflect the current iterate values.

The slab energy equation presented in Equation (4.24), is written in terms of temperature. However, the terms describing radiation heat transfer are a function of temperature to the fourth power. Rather than treat these terms explicitly, they are written as

$$\begin{aligned} Q_R &= A_{WF}\,\sigma\left[\sum_{m\epsilon\sigma_i} F_{im}\left(T_w^4 - T_{w_m}^4\right) + \sum_{n\epsilon\kappa_i} F_{in}\left(T_w^4 - T_{c_n}^4\right)\right] \\ &= A_{WF}\,\sigma\left[T_w^4\left(\sum_{m\epsilon\sigma_i} F_{im} + \sum_{n\epsilon\kappa_i} F_{in}\right) - \left(\sum_{m\epsilon\sigma_i} F_{im}\,T_{w_i}^4 + \sum_{n\epsilon\kappa_i} F_{in}\,T_{c_n}^4\right)\right] \\ &= A_{WF}\,\sigma\,H_{RAD}\,(T_w - \bar{T}) \end{aligned} \tag{4.49}$$

where $H_{RAD} = \epsilon_w T_w^3$

$$\bar{T} = \left(\sum_{m \epsilon \sigma_i} F_{im} T_{w_i}^4 + \sum_{n \epsilon \kappa_i} F_{in} T_{c_n}^4 \right) \Big/ \epsilon_w T_w^3$$

$$\epsilon_w = \left(\sum_{m \epsilon \sigma_i} F_{im} + \sum_{n \epsilon \kappa_i} F_{in} \right) .$$

When H_{RAD} and $\bar{T}$ are evaluated using current iterate values and this linear expression is substituted into the slab energy equation [Equation (4.24)], an equation that is linear in temperature at level j is obtained. These equations having this form for every slab at level j are combined to form the matrix equation

$$[U] \{T_w\}_j = \{S_w\} \tag{4.50}$$

where [U] is an NxN coefficient matrix (N being the number of slabs), $\{S_w\}$ is the source vector, and $\{T_w\}_j$ is the slab temperature at level j. For large problems the matrix [U] is sparse, therefore only the nonzero elements are stored.

The slab energy equation consists of terms containing not only slab temperatures, but also fluid temperatures, T_f, and composite radiation temperatures, $\bar{T}$. Fluid temperatures are obtained from the fluid energy equation and are represented in the source vector, $\{S_w\}$. After each fluid energy iteration, the source terms containing fluid temperatures are updated to reflect the current iterate values. The composite radiation temperature, $\bar{T}$, is derived as a summation of terms containing slab and clad temperatures to the fourth power. The clad portion of $\bar{T}$ is not updated during the fluid and slab solution. However, the slab portion of $\bar{T}$ is updated after every slab energy iteration.

Both the fluid and slab matrix equations are solved by successive over-relaxation with a default relaxation factor of 1.2. A single iteration consists of one sweep through the fluid equations followed by one sweep through the

slab equations. The iterate method continues until the changes in fluid enthalpy and slab temperature are both less than specified convergence criteria.

Once the fluid and slab energy solution has converged, the fluid temperatures are found using the fluid equation of state. The fluid temperatures are substituted into Equation (4.35) to obtain the rod cladding temperatures. If a detailed rod model is used, the fuel temperatures are back calculated using Equation (4.36).

For problems with several nodes and significant heat transfer in the radial direction, the energy solution may take hundreds of iterations to converge. To speed up the convergence rate, energy rebalancing is performed on both the fluid and slab matrix equations.

4.3 ENERGY CONSTITUTIVE MODELS

Constitutive relationships are required to close the system of equations described in the previous sections. For example, heat transfer coefficients are used to describe convection heat transfer and are required to close all three energy equations. The constitutive models presented below are empirical in nature and, therefore, should be applied with care since they may be valid only over a certain range of conditions.

4.3.1 Nusselt Number Correlations

The convection heat transfer coefficient is calculated using a Nusselt number, Nu, from the expression

$$H = Nu\ k/D_h \tag{4.51}$$

where k is the fluid conduction and D_h is the hydraulic diameter of the channel. The Nusselt number is obtained from the expression

$$Nu = A\ Re^a Pr^b + B \tag{4.52}$$

where Re is the subchannel Reynolds number, defined as

$$Re = \frac{mD_h}{A\mu} \tag{4.53}$$

and Pr is the fluid Prandtl number. Two correlations can input for each channel type and the largest of the two, based on local Reynolds and Prandtl number, is used for computing the heat flux.

4.3.2 Fluid Conduction Shape Factor

The fluid conduction heat flux between adjacent channels is characterized by the gap width, S, and a conduction length, ℓ_c, defined as

$$\ell_c = \ell/GK \tag{4.54}$$

where ℓ is the transverse momentum control volume length and GK is an empirically determined conduction shape factor. Doubling the value of GK effectively doubles the radial fluid-to-fluid conduction heat transfer. Note that $1/GK = Z_k$ is used in the fluid energy Equation (4.13). The optimal value of GK is very problem dependent. Experience has shown that for light water fuel assemblies, GK should be chosen to make ℓ_c approximately equal to the subchannel centroid-to-centroid distance.

4.3.3 Solid-to-Solid Conductances

The solid conduction between adjacent slabs is modeled using a composite thermal conductance, U, which includes the heat transfer area, the thermal conductivity of the slab materials and any gap resistance or thermal radiation at the slab interface. The components that make up the total thermal resistance between two adjacent slab nodes are shown in Figure 4.7. The terms R_1 and R_2 denote the thermal resistances from the center of the slab to the slab interface and account for the slab geometry and material conductivity. The total series resistance from the slab material is

$$R_{SOL} = R_1 + R_2 \tag{4.55}$$

where R = L/Ak and L is the conduction length and k is the thermal conductivity of the solid node. This is the total resistance between two slabs unless there is a gap at the slab interface.

Heat may be transferred across a gap between the two slabs by conduction through the fluid or by thermal radiation. The radiation heat transfer is modeled using an approximate thermal resistance for radiation between gray parallel plates, given by

$$R_{RAD} = \frac{1/\epsilon_1 + 1/\epsilon_2 - 1}{4\,\sigma\,A\,(T_1^2 + T_2^2)(T_1 + T_2)} \tag{4.56}$$

where T_1 and T_2 are in degrees Rankine and ϵ_1 and ϵ_2 are the surface emissivities of the two slabs. This resistance, along with the thermal resistance for conduction through fluid in the gap, is used to calculate a total gap thermal resistance using the expression

$$R_{GAP} = \frac{1}{R_{RAD}} + \frac{1}{R_{CON}} \tag{4.57}$$

The overall thermal conductance between adjacent slabs, U, is given by

$$U = \frac{1}{R_{SOL} + R_{GAP}} \tag{4.58}$$

4.3.4 Radiation Exchange Factors

The radiation heat transfer between rod and slab surfaces is modeled using radiation exchange factors. The net rate of radiant energy outflow from surface i to surface j, Q_{ij}, is defined in terms of an exchange factor, F_{ij}, as

$$Q_{ij} = A_i\,F_{ij}\sigma\,(T_i^4 - T_j^4) \tag{4.59}$$

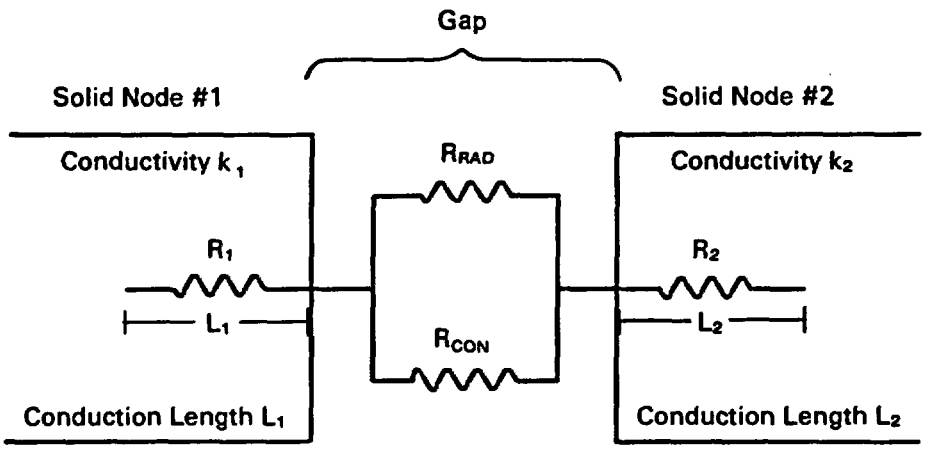

FIGURE 4.7 Solid-to-Solid Resistance Network

The quantity F_{ij} specifies the fraction of the total amount of radiant energy emitted from surface i that reaches surface j and is absorbed. This includes all the paths by which radiation may reach surface j from surface i, including the direct path and paths of single or multiple reflections. This differs from the blackbody view factor, F_{ij}, which does not account for reflections. For all black surfaces ($\epsilon = 1.0$), the two quantities are the same.

The radiation exchange factors, F_{ij}, are calculated from the geometry of the problem and the emissivities of the participating surfaces using the following set of equations (Cox 1977).

$$\sum_{i=1}^{n} \left[F_{ki} \left(\frac{1-\epsilon_i}{\epsilon_i} \right) - \frac{\delta_{ki}}{\epsilon_i} \right] F_{ij} = - F_{kj}\epsilon_j ; j = 1,\ldots,n;\ k = 1,\ldots,n. \quad (4.60)$$

where F_{ki} and F_{kj} are the blackbody view factors, ϵ_i is the emissivity of surface i, δ_{ki} is the Kronecker delta, and n is the number of surfaces in an enclosure.

The radiation exchange factors used in the COBRA-SFS code can be obtained in two different ways. For radiation enclosures that do not involve a rod assembly, the blackbody view factors and surface emissivities are read directly into the input and radiation exchange factors calculated within COBRA-SFS. For radiation enclosures that include a rod assembly, the radiation exchange factors are read from a separate input. An auxilliary computer code, RADX-1, is used to generate the blackbody view factor array and to calculate the radiation exchange factors for unconsolidated spent fuel assemblies. This method is described in detail in the Appendix.

4.4 THERMAL BOUNDARY CONDITIONS

To solve the system of energy equations described in the previous sections, thermal boundary conditions must be specified. A typical COBRA-SFS model consists of three regions: an upper plenum, the channel region, and a lower plenum. For the channel region, thermal boundary conditions are applied to the outer solid structure nodes at each axial level. Boundary conditions for the plenum regions are applied in the axial and radial directions for both plenums. The expression for heat transfer used in these boundary conditions may include conduction, thermal radiation, and/or natural convection. The side thermal boundary conditions are described in Section 4.4.1. The thermal boundary conditions for the plenum regions are described in Section 4.4.2.

4.4.1 Side Boundary Conditions

The fluid and solid structure and fuel rod energy equations for the channel region were developed in Section 4.1. When no side thermal boundary conditions are specified, the outside boundary at each axial level is assumed to be adiabatic. A boundary condition is specified when heat is to be transferred to some specified boundary temperature.

At each axial level, a one-dimensional thermal connection is made between each outside surface node and a boundary temperature. Each connection may consist of one or a series of radial "regions", with each region having a different expression for heat transfer. The heat transfer rate through each region is expressed in the form

$$q''_{boundary} = C_1 \left[C_2 \left(T_i - T_{i+1}\right)^{C_3} \right] \left(T_i - T_{i+1}\right) + \sigma \left(\frac{1}{\epsilon_i} + \frac{1}{\epsilon_{i+1}} - 1 \right)^{-1} \left(T_i^4 - T_{i+1}^4 \right) \quad (4.61)$$

where

C_n = user defined constants

T_i = temperature for boundary region i

σ = Boltzmanns' constant

ϵ_i = surface emissivity for boundary region i.

This expression is more general than those used in the energy equations described in Section 4.1 in that it allows the modeling of heat transfer modes that are not linear in temperature (such as natural convection, that is expressed in terms of a Grashof or Rayleigh number).

Boundary temperatures are input as a set of axial profiles that are assigned to each solid structure node at the boundary. In this way, the boundary temperatures can vary both axially and circumferentially.

Before the rod, fluid, and slab energy equations at any axial level are solved, the temperatures in the boundary regions are estimated using slab temperatures from the previous iteration. The one-dimensional series of equations for each boundary connection is solved iteratively for a radial temperature distribution in the boundary region. After the boundary solution has converged, a linear composite resistance is constructed to represent the total connection between the outermost slab node and the specified boundary temperature. This resistance and the boundary temperature are then implemented in the solid structure energy equation [Equation (4.24)]. After all boundary

resistances at an axial level have been computed, the energy equations for that level are solved.

4.4.2 Plenum Boundary Conditions

In a COBRA-SFS cask model, the fluid in a hot assembly flows upward until it enters the upper plenum region at the top of the cask. The flow is then assumed to mix with all the other fluid entering the plenum. Heat is lost to the environment through the top and sides of the plenum region. The fluid then flows downward through the cooler assemblies until it reaches the lower plenum.

The plenum regions are only used in problems where flow recirculation occurs. The primary purpose of the plenum model is to determine the enthalpy of fluid returning to the channel region.

Each plenum has an axial and radial one-dimensional thermal connection between the fluid in the plenum and a boundary temperature. Different boundary temperatures may be specified for each direction. The connection, similar to that used in the side boundary specification, may consist of one or a series of "regions", with each region having a different expression [Equation (4.62)] for heat transfer. In addition, each plenum region can have thermal connections to solid structure nodes of the channel region in the axial level adjacent to the plenum. These connections are used to represent axial heat transfer from the cask body or heat transfer from the basket to the bottom or top of the cask.

The fluid enthalpies and flow rates entering the plenum as well as temperatures of the solid structure nodes connected to the plenum are computed in the energy solution for the axial level adjacent to the plenum. These values are then held fixed while the plenum equations are solved iteratively. The resulting plenum structure temperatures and plenum fluid enthalpy are held fixed for the next iteration of the rod, fluid, and slab energy solution.

5.0 REFERENCES

Cox, R. L. 1977. Radiation Heat Transfer in Arrays of Parallel Cylinders. ORNL-5239, Oak Ridge National Laboratory, Oak Ridge, Tennessee.

Cuta, J. M. and J. M. Creer. 1986. "Comparisons of COBRA-SFS Calculations to Data from Electrically Heat Test Sections Simulating Unconsolidated and Consolidated BWR Spent Fuel", EPRI-NP-4593, Electric Power Research Institute, Palo Alto, California.

George, T. L., et al. 1980. COBRA-WC: A Version of COBRA for Single-Phase Multiassembly Thermal-Hydraulic Transient Analysis. PNL-2359, Pacific Northwest Laboratory, Richland, Washington.

Gosman, A.D., R. Herbert, S. V. Patankor, R. Potter and D. B. Spalding. October 1973. The SABRE Code for Prediction of Coolant Flows and Temperatures in Pin Assemblies Containing Blockages. Report HTS/73/47, Imperial College of Science and Technology. (Presented at International Meeting on Reactor Heat Transfer, Karlsruhe.)

Hirt, C. W. and J. L. Cook. 1972. "Calculating Three-Dimensional Flows Around Structures and Over Rough Terrain." Journal of Computational Physics, Vol. 10, pp. 324-340.

Ingesson, L. and S. Hedberg. 1970. "Heat Transfer Between Subchannels in a Rod Assembly." Paper No. FC7.11. Presented at 4th International Heat Transfer Conference, Versailles, FRANCE.

Lombardo, N. J., J. M. Cuta, T. E. Michener, D. R. Rector, and C. L. Wheeler. 1986. COBRA-SFS: A Thermal-Hydraulic Analysis Computer Code; Volume III - Validation Assessments. PNL-6049, Pacific Northwest Laboratory, Richland, Washington.

Rector, D. R., J. M. Cuta, N. J. Lombardo, T. E. Michener, and C. L. Wheeler. 1986a. COBRA-SFS: A Thermal-Hydraulic Analysis Computer Code; Volume II - User's Manual. PNL-6049, Pacific Northwest Laboratory, Richland, Washington.

Rector, D. R., R. A. McCann, U. P. Jenquin, C. M. Heeb, J. M. Creer, and C. L. Wheeler. 1986b. CASTOR-1C Spent Fuel Storage Cask Decay Heat, Heat Transfer, and Shielding Analysis. PNL-5974, Pacific Northwest Laboratory, Richland, Washington.

Rogers, J. T., and N. E. Todreas. 1968. "Coolant Mixing in Reactor Fuel Rod Assemblies--Single-Phase Coolants." Heat Transfer in Rod Assemblies. ASME pp. 1-56.

Rogers, J. T., and R. G. Rosehart. 1972. "Mixing by Turbulent Interchange in Fuel Assemblies, Correlations and Inferences." ASME Paper No. 72-Ht-53.

Rowe, D. S. March 1973. COBRA-III C: A Digital Computer Code for Steady-State and Transient Thrmal Hydraulic Analysis of Rod Assembly Nuclear Fuel Elements. BNWL-1695, Pacific Northwest Laboratory, Richland, Washington.

Stewart, C. W., et al. 1977. COBRA-IV: The Model and the Method. BNWL-2214, Pacific Northwest Laboratory, Richland, Washington.

Tong, L. S. 1968. "Pressure Drop Performance of a Rod Assembly." In Heat Transfer in Rod Assemblies. ASME, pp. 57-69

Wheeler, C. L., et al. March 1976. COBRA-IV-I: An Interim Version of COBRA for Thermal Hydraulic Analysis of Rod Assemblies, Nuclear Fuel Elements and Cores. BNWL-1962, Pacific Northwest Laboratory, Richland, Washington.

Wiles, L. E., N. J. Lombardo, C. M. Heeb, U. P. Jenquin, J. M. Creer, C. L. Wheeler, and R. A. McCann. 1986. BWR Spent Fuel Storage Cask Performance Test: Volume II - Pre- and Post-Test Decay Heat, Heat Transfer, and Shielding Analyses. PNL-5777, Vol. II, Pacific Northwest Laboratory, Richland, Washington.

APPENDIX

RADX-1: RADIATION EXCHANGE FACTOR GENERATOR

APPENDIX

RADX-1: RADIATION EXCHANGE FACTOR GENERATOR

The thermal radiation models used in the solid structure and fuel rod energy equations require a set of radiation exchange factors, F_{ij}, which describe the net amount of energy transferred from each surface to every other surface in an enclosure. For simple enclosures with relatively few surfaces, the required blackbody viewfactors and surface emissivities may be input directly by the user. However, for a rod assembly with hundreds of radiation surfaces, this would be an extremely arduous task. For this reason, a support computer code, RADX-1, was developed to generate radiation exchange factors for rods in unconsolidated square arrays.

The net rate of radiant energy outflow from surface i to surface j, Q_{ij}, is defined in terms of an exchange factor, F_{ij}, as

$$Q_{ij} = A_i F_{ij} \sigma (T_i^4 - T_j^4) \tag{4.59}$$

The quantity F_{ij} specifies the total amount of radiant energy emitted from surface i that reaches surface j and is absorbed. This includes all the paths by which radiation may reach surface j from surface i, that is, the direct path, paths by means of one reflection, and paths by multiple reflections. This differs from the blackbody view factor, F_{ij}, which does not account for reflections. For all black surfaces ($\epsilon = 1.0$), the two quantities are the same.

The radiation exchange factors, F_{ij}, are calculated from the geometry of the problem and the emissivities of the participating surfaces using the set of equations (Cox 1977)

$$\sum_{i=1}^{n} F_{ki} \frac{1-\epsilon_i}{\epsilon_i} - \frac{\delta_{ki}}{\epsilon_i} F_{ij} = - F_{kj}\epsilon_j; j = 1,\ldots,n;\ k = 1,\ldots,n. \tag{4.60}$$

where F_{ki} is the blackbody view factor, ϵ_i is the emissivity of surface i, and n is the number of surfaces in the enclosures. The following assumptions were made in developing this equation:

1) nonparticipating media
2) isothermal, gray surfaces
3) reflected and emitted radiation is diffusely distributed
4) uniform radiosity over each defined surface.

The accuracy of the radiation model that uses radiation exchange factors, F_{ij}, is affected by how the enclosure is divided into surfaces. For example, if a fuel rod is modeled using a single surface, radiation received on one side of a rod is reflected evenly around the rod. For this reason, rod surfaces are divided into quarters to provide a more physically representative model for the radiation exchange calculations.

The viewfactor model for a typical square array rod assembly is shown in Figure A.1. All rods are divided into four surfaces and the surrounding canister is divided into eight surfaces. By adding three rows of pseudo rods to each side of the actual rod array, the surrounding solid surfaces are approximated without requiring a geometry specific wall model. When a blackbody viewfactor extends to one of these pseudo rods, its contribution is included as part of a solid surface.

A set of blackbody viewfactors from each quarter rod to other quarter rods is developed for use in Equation (4.60). Figure A.2 shows the distribution of viewfactors for each quarter rod. A total of fifteen surfaces are "seen" by an originating surface. The furthest surface that can directly receive radiation is assumed to be three rows from the originating surface. The expressions used to calculate the blackbody viewfactors from the originating surface to each of the other surfaces are presented in Table A.1. The calculated viewfactor from the originating surface to the outermost surface, h, includes the viewfactors to all the surfaces beyond surface h. The expressions for the base viewfactors were developed using Hottel's cross-string method (Cox 1977) and were written for pitch-to-diameter ratios in the range of $< 1 \leq \text{PDR} \leq \sqrt{2}$.

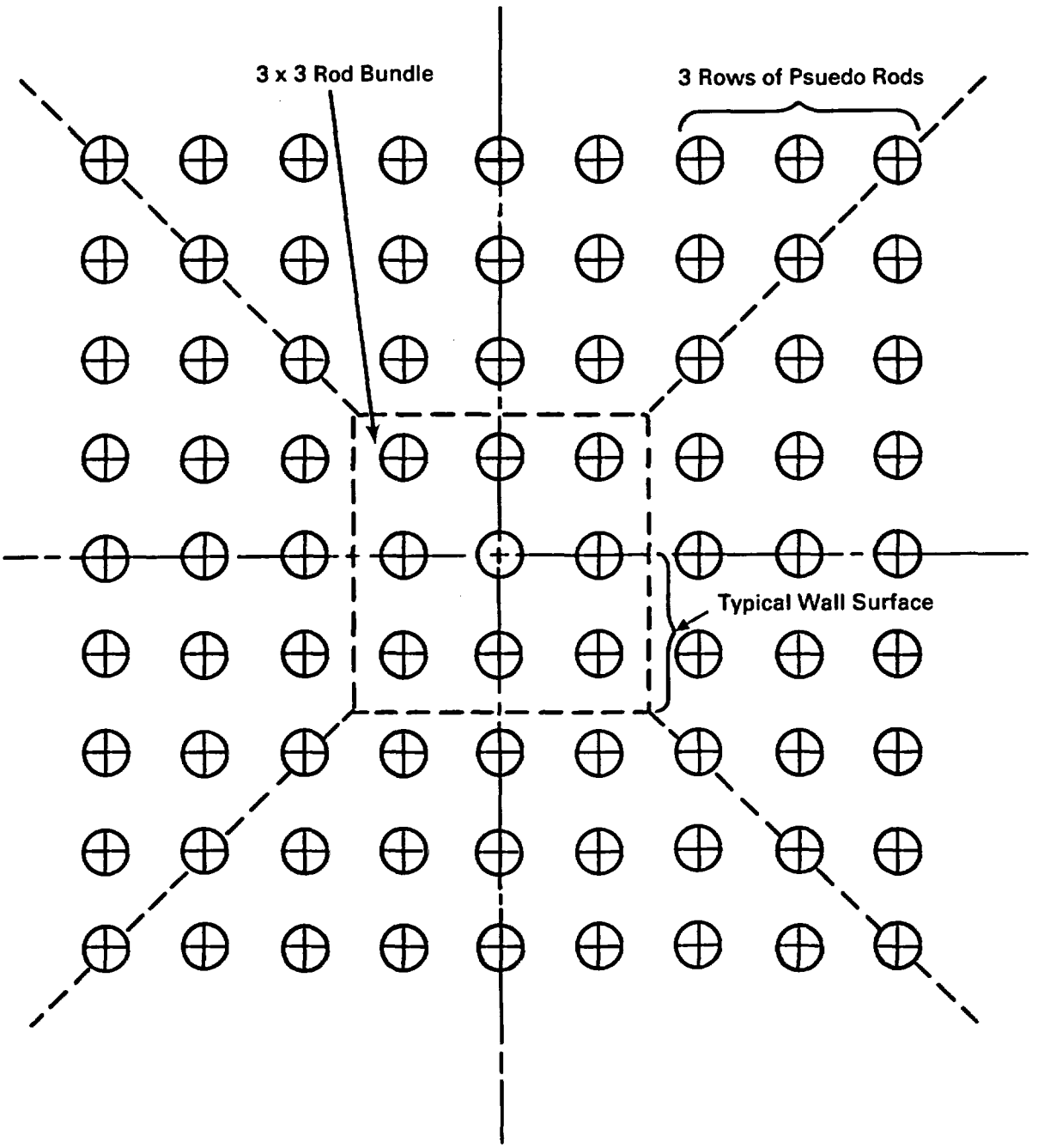

FIGURE A.1. Viewfactor Model for a Typical Rod Assembly (3 X 3)

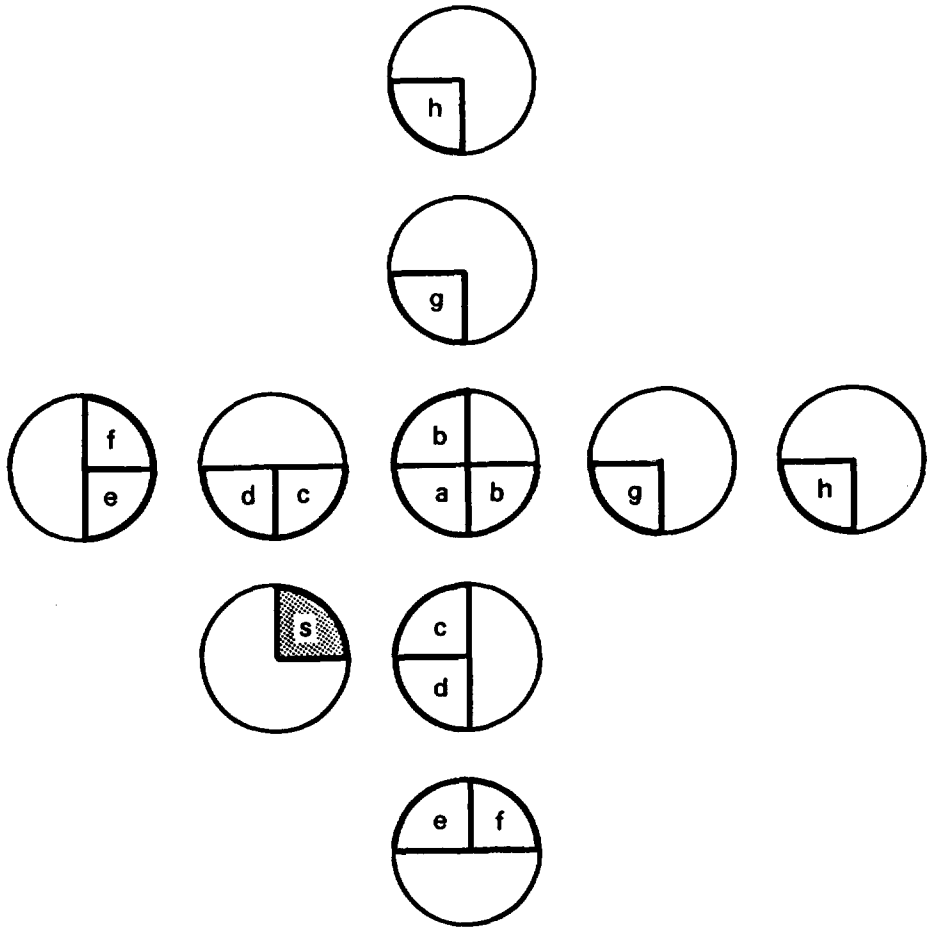

FIGURE A.2. Blackbody Viewfactor Distribution for Each Quarter Rod

TABLE A.1. Quarter Rod Blackbody Viewfactor Expressions

Blacbody Viewfactor	Expression[a]
F_{s-a}	$4/\pi \{(2PDR^2 - 2PDR+1)^{0.5} - (2PDR^2 - 2PDR + 0.5)^{0.5}\}$
F_{s-b}	$2/\pi \{(2PDR^2 - 2PDR + 0.5)^{0.5} - (2PDR^2 - 2PDR + 1)^{0.5} -ATAN [(PDR-0.5)/PDR] + \pi/4\}$
F_{s-c}	$2/\pi \{(PDR^2 - PDR)^{0.5} - ATAN [2(PDR^2 - PDR)^{0.5}] - PDR + 1 + \pi/2\}$
F_{s-d}	$2/\pi \{(PDR^2 - 1)^{0.5} - 2(PDR^2 - PDR)^{0.5} + ATAN [2(PDR^2 - PDR)^{0.5}] - ATAN [PDR^2 - 1)^{0.5}] + PDR - 1\}$
F_{s-e}	Same as F_{s-b}
F_{s-f}[b]	$2/\pi \{2 (2PDR^2 - PDR)^{0.5} - (2PDR^2 - 2PDR + 0.5)^{0.5} - 2 (PDR^2 - 1)^{0.5} + ATAN [(PDR - 0.5)/PDR] - ATAN [2(2PDR^2 - PDR)^{0.5}] + 2 ATAN [(PDR^2 - 1)^{0.5}] - \pi/4\}$
F_{s-g}	$2/\pi \{(5PDR^2 - 1)^{0.5} - ATAN [(5PDR^2 - 1)^{0.5}] - 2(2PDR^2 - 1)^{0.5} - ATAN [(2PDR^2 - 1)^{0.5}] + (PDR^2 - 1)^{0.5} - ATAN [(PDR^2 - 1)^{0.5}] - ATAN (0.5)\}$
F_{s-h}	$1/2 \{1-F_{s-a} - 2 [F_{s-b} + F_{s-c} + F_{s-d} + F_{s-e} + F_{s-f} + F_{s-g}]\}$

(a) PDR = pitch-to-diameter ratio ($1 < PDR \leq \sqrt{2}$)
(b) For this viewfactor only, PDR > 1.254

When a complete set of blackbody viewfactors and surface emissivities are used in Equation (4.61), a set of n^2 equations result. These equations are solved iteratively using successive overrelaxation.

After solving the n^2 equation set, the resulting set of quarter rod gray body exchange factors are combined to obtain full rod gray body exchange factors. The exchange factors are combined so that the total heat transferred from rod i to rod j, Q_j, is equal to the sum of heat transfer from each quarter rod, n, of rod i to each quarter rod, m, of rod j

$$Q_{ij} = \sum_{n=1}^{4} \sum_{m=1}^{4} Q_{nm} \tag{A.1}$$

The heat transferred from one quarter rod to another by radiation is given by

$$Q_{nm} = A\sigma F_{nm} (T_n^4 - T_m^4) \tag{A.2}$$

Where F_{nm} are the quarter rod exchange factors. Assuming that rods i and j are isothermal, the total heat transfer from rod i to rod j is written as

$$Q_{ij} = \sum_{n=1}^{4} \sum_{m=1}^{4} \Delta x \frac{\pi d}{4} \sigma F_{nm} (T_i^4 - T_j^4)$$

$$= \Delta x \frac{\pi d}{4} \sigma (T_i^4 - T_j^4) \sum_{n=1}^{4} \sum_{m=1}^{4} F_{nm} \tag{A.3}$$

The total heat transfer from rod i to rod j is defined as

$$Q_{ij} = A \sigma F_{ij} (T_i^4 - T_j^4) \tag{4.59}$$

Equating equations (A.3) and (4.60), the rod-to-rod radiation exchange factor F_{ij} is

$$F_{ij} = \frac{1}{4} \sum_{n=1}^{4} \sum_{m=1}^{4} F_{nm} \qquad \text{(A.4)}$$

Depending on the symmetry of the problem, the full rod exchange factors for the full assembly may be "folded" or combined to give a set of exchange factors for a symmetric half or eighth sector of an assembly. The final set of exchange factors are output to a file to be used as input to the COBRA-SFS code. This approach allows one to use a model in COBRA-SFS that assumes an isothermal rod surface temperature while allowing the radiosity to vary around the rod.

PNL-6049
UC-85

DISTRIBUTION

No. of Copies

OFFSITE

110 DOE Technical Information Center

R. Bown
U.S. Department of Energy
Office of Civilian Radioactive Waste Managment
RW-30
Washington, DC 20545

J. Epstein
U.S. Department of Energy
Office of Civilian Radioactive Waste Managment
RW-30
Washington, DC 20545

J. R. Hilley
U.S. Department of Energy
Office of Storage and Transportation Systems
Washington, DC 20545

D. E. Shelor
U.S. Department of Energy
Office of Civilian Radioactive Waste Management
RW-32
Washington, DC 20545

H. Steinburg
U.S. Department of Energy
Office of Storage and Transportation Systems
RW-33
1000 Independence Ave
Washington, DC 20545

No. of Copies

W. Stringfield
U.S. Department of Energy
Office of Civilian Radioactive Waste Management
Washington, DC 20545

R. E. Steins
U.S. Department of Energy
Idaho Operations Office
550 2nd Street
Idaho Falls, ID 83401

K. G. Golliher
U.S. Department of Energy
Albuquerque Operations Office
P.O. Box 5400
Albuquerque, NM 87115

L. Lanni
U.S. Department of Energy
Magnetic Fusion and Energy Divsion
San Francisco Operations Office
1333 Broadway
Oakland, CA 94612

C. Matthews
U.S. Department of Energy
Oak Ridge National Laboratory
P.O. Box E
Oak Ridge, TN 37830

D. Veith
U.S. Department of Energy
Nevada Operations Office
P.O. Box 14100
Las Vegas, NV 83114

No. of
Copies

N. H. Davison
U.S. Nuclear Regulatory
Commission
Office of Nuclear Materials
Safety and Safeguards
Washington, DC 20555

C. Feldman
U.S. Nuclear Regulatory
Commission
Office of Nuclear Regulatory
Research
MS 5650 NL
Wasington, DC 20555

W. Lake
U.S. Nuclear Regulatory
Commission
Office of Nuclear Materials
Safety and Safeguards
Wasington, DC 20555

C. H. Peterson
U.S. Nuclear Regulatory
Commission
Office of Nuclear Materials
Safety and Safeguards
MS 62355
Wasington, DC 20555

J. A. Carr
Battelle Memorial Institute
Office of Nuclear Waste
Isolation
505 King Avenue
Columbus, OH 43201

B. A. Rowles
Battelle Memorial Institute
Office of Nuclear Waste
Isolation
505 King Avenue
Columbus, OH 43201

No. of
Copies

R. Kunita
Carolina Power & Light Co.
P.O. Box 1551
Raleigh, NC 27602

C. K. Anderson
Combustion Engineering, INc.
1000 Prospect Hill Road
Windsor, CT 06095

V. Walker
Ebasco Services Incorporated
Two World Trade Center
New York, NY 10048

D. H. Schoonen
EG&G
P.O. Box 1625
Idaho Falls, ID 83415

P. E. Eggers
Eggers Ridihalgh Partners, Inc.
1445 Summit Street
Columbus, OH 43201

FLUOR Engineers, Inc.
Advanced Technology Division
P.O. Box C-11944
Santa Anna, CA 92711-1944

E. E. Volland
General Electric Company
Nuclear Fuel & Services
Divsion
7555 E. Collins Road
Morris, IL 60450

R. Anderson
General Nuclear Services, Inc.
135 Darling Drive
Avon, CT 06001

No. of
Copies

L. B. Ballou
Lawrence Livermore National
Laboratory
P.O. Box 808
Livermore, CA 94550

M. W. Schwartz
Lawrence Livermore National
Laboratory
P.O. Box 808
Livermore, CA 94550

C. E. Walter
Lawrence Livermore National
Laboratory
P.O. Box 808
Livermore, CA 94550

H. Lowenburg
Lowenburg Associates
1091 Rosemont Drive
Rockville, MD 20852

J. Houston
Nuclear Assurance Corporation
5720 Peach Tree Parkway
Norcross, GA 30092

R. T. Haelsig
Nuclear Packaging Inc.
1010 S. 336th Street
Federal Way, WA 98003

L. E. Wiles
Numerical Applications, Inc.
825 Goethals Drive
Richland, WA 99352

J. V. Massey
NUTECH Engineers
145 Martinvale Lane
San Jose, CA 95116

No. of
Copies

C. V. Parks
Oak Ridge National Laboratory
P.O. Box X
Oak Ridge, TN 37831

D. Woods
Ralph M. Parson Co.
100 West Walnut Street
Pasadena, CA 91124

T. L. Sanders
Sandia National Laboratory
Albuquerque, NM

M. E. Mason
Transnuclear, Inc.
1 N. Broadway
White Plains, NY 10601

TRW, Inc.
Energy Development Group
Suite 201
200 Union Blvd.
Denver, CO 80228

C. E. King
Uranium Mgt. Corp.
175 Curtner Ave. MC 620
San Jose, CA 95125

M. L. Smith
Viriginia Electric Power Co.
P.O. Box 26666
Richmond, VA 23261

K. L. Basehore
Virginia Electric Power Co.
Power Station Engineering
The Electric Building
P.O. Box 564
7th and Franklin
Richmond, VA 23204

No. of
Copies

D. L. Larkin
Washington Public Power Supply System
P.O. Box 968
Richland, WA 99352

R. O. Anderson
Northern States Power Company
15 S. 15th Street
Minneapolis, MN 55401

G. Swindlehurst
Duke Power Company
P.O. Box 33189
422 S. Church Street
Charlotte, NC 28242

D. Hamilton
Middle South Services, Inc.
Box 61000
New Orleans, LA 70161

G. R. Bond
Manager, Nuclear Fuels
General Public Utilities-NUC
100 Interpace Parkway
Parsippany, NJ 07054

J. R. Ratliff
Tennessee Valley Authority
409 Krystal Building
Chattanooga, TN 37401

B. Rice
Texas Utilities Generating Co.
Skyway Tower
400 North Olive Street
LB81
Dallas, TX 75201

No. of
Copies

R. K. Van Galder
Associate Engineer
Long Island Light Company
175 E. Old Country Road
Hicksville, NY 11801

H. E. Bliss
Nuclear Fuel Services
Commonwealth Edison
72 West Adams Street
P.O. Box 767
Chicago, IL 60690

R. T. Harris
Northeast Utilities
P.O. Box 270
Hartford, CN 06101

A. Ladieu
Yankee Atomic Electric Company
1671 Worcester Road
Framingham, MA 01701

D. S. Rowe
Rowe and Associates
14400 Bellevue-Redmond Road, Suite 208
Bellevue, WA 98007

E. U. Khan
U.S. Department of Energy
Headquarters
Office of Space Reactor Projects
19901 Germantown Road
Germantown, MD 20874

Y. Hsii
Division of Systems Integration
Office of Nuclear Reactor Regulation
U.S. Nuclear Regulatory Commission
Wasington, DC 20555

No. of
Copies

L. Phillips
Division of Systems Integration
Office of Nuclear Reactor Regulation
U.S. Nuclear Regulatory Commission
Wasington, DC 20555

L. Agee
Electric Power Research Inst.
P.O. Box 10412
Palo Alto, CA 94303

R. W. Lambert
Electric Power Research Inst.
P.O. Box 10412
Palo Alto, CA 94303

G. S. Srikantiah
Electric Power Research Inst.
P.O. Box 10412
Palo Alto, CA 94303

R. Rice
EG&G Idaho, Inc.
P.O. Box 1625
Idaho Falls, ID 83415

J. H. Saling
Westinghouse Electric Corp.
Waste Technology Services Division
P.O. Box 10864
Pittsburg, PA 15236

Dr. Dale Klein
Mechanical Engineering Dept.
University of Texas
Austin, TX 78712

B. A. Chin
Mechanical Engineering Dept.
247 Wilmore Labs
Auburn University, AL 36849

No. of
Copies

ONSITE

2 DOE Richland Operations Office

R. D. Izatt
J. P. Collins

3 Rockwell Hanford Operations

M. B. Arndt
C. L. Brown
G. T. Harper

40 Pacific Northwest Laboratory

G. H. Beeman
J. M. Cuta
J. M. Creer (10)
C. M. Heeb
A. B. Johnson, Jr.
B. M. Johnson
D. K. Kreid
N. J. Lombardo
R. A. McCann
T. E. Michener
D. R. Rector (10)
C. W. Stewart
R. A. Stokes
D. S. Trent
C. L. Wheeler
Technical Library (5)
Publishing Coordination (2)

2 HEDL

R. Einziger
R. Stover